Nonlinear Dyn (2022) 108:141–166
https://doi.org/10.1007/s11071-022-07223-x

ORIGINAL PAPER

Nonlinear dynamic analysis of variable lead preloaded single nut ball screw considering the variation of working parameters

Zhendong Liu · Mengtao Xu · Hongzhuang Zhang · Changyou Li · Guo Yao · Zhenyuan Li · HuiHui Miao · Chenyu Wang · Yimin Zhang

Received: 14 June 2021 / Accepted: 8 January 2022 / Published online: 24 January 2022

Abstract In this study, a five-degree-of-freedom dynamic model of variable lead preloaded single nut ball screw is proposed. The proposed model considers the effect of excitation amplitude, deflection angle, the number of balls, and the preload into consideration. Moreover, to study the effect of working parameters on nonlinear dynamics, bifurcation diagram, 3-D frequency spectrum, phase diagram, and Poincaré section with different system parameters are shown in the Discussion section. The numerical analysis indicates that the system can exhibit different motion states, and the continuous frequency component can be observed. Moreover, a series of experiments are conducted to estimate the dynamic parameters and validate the proposed dynamic model.

Keywords Single nut ball screw · Nonlinear dynamics · Working parameters

Z. Liu · M. Xu · H. Zhang · C. Li (✉) · G. Yao (✉) · Z. Li · H. Miao · C. Wang
School of Mechanical Engineering and Automation, Northeastern University, Shenyang 110819, China
e-mail: chyli@mail.neu.edu.cn

G. Yao
e-mail: yaoguo@me.neu.edu.cn

Y. Zhang
College of Mechanical and Automotive Engineering, Zhaoqing University, Zhaoqing 526061, China

1 Introduction

Ball screws have been used in missiles and aircraft to move control surface [1]. It is also used in machine tools, robots, and many other precision assembly equipment pieces due to its high efficiency, great stiffness, and long service life [2]. The positioning accuracy of ball screw feed system is usually influenced by preload [3], thermal deformation [4], and health condition of each kinematic joint [5]. During the positioning process, the precision of the feed system can be strongly affected by working condition, manufacturing accuracy, and assembly quality. Due to the nonlinear Hertzian contact stress, piecewise restoring force, and deflection angle, the system can exhibit a wide variety of nonlinear dynamics. However, the influence of assembly error on nonlinear dynamic characteristic has been discussed by few papers. In addition, the preload can be changed with the increase in service life. Therefore, it is necessary to study the nonlinear behavior of ball screw feed system to avoid the reduction in positioning accuracy under the complex working conditions. The dynamic characteristics of ball screw have been studied by many researchers under different conditions.

Liu et al. [6] proposed a nine-degree-of-freedom dynamic model of ball screw feed system, the effect of assembly error on the nonlinear dynamics of the system was discussed, and the screw nut in the proposed model had three degrees of freedom.

However, the screw nut was also subjected to torsional moment, and the moment should not be ignored. Guo and Yi [7] investigated the relationship between the detected vibration signals and the variation of preload and developed a lumped dynamic model to study the preload variation of the ball screw feed system. Bo et al. [8] developed a mathematical model to predict the structural nature frequency influenced by moving component. Considering the influences of dimension errors of balls in screw nut, Ni and Qi [9] proposed a calculation model to analyze the effect of ball's dimension error on mechanical properties of a ball screw drive system, and the fatigue life influenced by ball's machining accuracy was studied. Chen and Tang [10] found that the force of each ball was not same and developed stiffness transition matrices for the ball screw mechanism to study the influence of the contact stiffness. Due to the large friction force, the contact state of each component could change and hence influenced the dynamic characteristics of the ball screw feed system. Using hybrid element method, Zhang et al. [11] theoretically investigated the relationship between ball screw feed system natural frequency and feed rates and pointed out that the resonance may occur when the natural frequency of the feed system was near the torque ripple harmonic frequency of the motor. Dong and Tang [12] established a hybrid model to study the structural dynamics of the ball screw drive and analyzed the axial, torsional, and flexural dynamic behaviors of ball screw feed system by using the method of continuous beam. Wang et al. [13] developed a time-varying dynamic model to investigate the vibration characteristics of multi-degree-of-freedom feed system, the restoring force of screw nut was considered as a piecewise function, and the coupling effects of screw nut position and excitation amplitude were investigated by simulation. Xu et al. [14] presented an analytical restoring force function to study the effect of sliding platform position, external excitation, and nominal contact angles. Moreover, the dynamic response of the system is discussed. High acceleration could cause the large inertial force of the moving components, which lead to the change of the contact stiffness, and bring influence to the dynamic behaviors of the ball screw feed system. Considering the effect of acceleration, Zhang et al. [15] proposed an equivalent dynamic model using lumped parameter method and derived the equivalent axial stiffness of screw nut based on the contact state which is influenced by the variation of inertial force. Moreover, it pointed out that the return tube of a ball screw-driven mechanism has been designed to provide the path for balls rolling in screw nut grooves. Due to the complexity of working environment, the return tube might damage which is caused by high excitation frequency and excitation amplitude. Huang et al. [16] developed an impact–contact formula for the feed system and investigated the transient behavior using finite element method. Due to the complexity of working condition, the contact angle of angular contact ball bearing was not a constant value. Liao and Lin [17] established a three-dimensional expression of balls based on the geometry parameters at different position angles and discussed the effect of radial and axial deformation on the contact deformation, normal force, and contact angle. Due to the machining error, assembly error, and complicated working condition, the distribution of the load distribution of ball screws was unbalanced. Liu et al. [18] established an appropriate transformation coordinate system to analyze the static load distribution of ball nut. Moreover, the effect of initial contact angle and axial load was discussed in detail. In order to analyze the contact load of balls in screw nut when there exists a turning torque caused by an assembly error, Zhao et al. [19] establish a load distribution model. Furthermore, the effect of the elastic creep on transmission accuracy was studied. As the sliding wear of ball nut was the main reason which caused the decrease in preload. Wei et al. [20] proposed a two-body abrasion model to study the variations of wear depths in the axial direction which are directly related to the preload of screw nut. Okwudire and Altintas [21] analytically and experimentally proved that the lateral dynamics of the ball screw feed system could affect the positioning accuracy under the condition of high acceleration. Considering the influence of the deformation of the screw nut and geometry error, Zhou et al. [22] proposed a modified load distribution model. In addition, an experiment was conducted to validate the proposed model. As the increase in velocity and acceleration of the ball screw drives the system, the resonant of the system may degrade the positioning accuracy. Diego et al. [23] developed a high-frequency dynamic model of a ball screw drive feed system. Simultaneously, the frequency variation with different worktable position was studied. Kolar et al. [24] investigated the effect of frame properties on

the dynamic characteristics and conducted a cutting experiment to validate the simulation result. To reduce the impact of thermal error and control vibration, lots of theoretical analysis and experimental research had been done by many researchers [25–28]. Wang et al. [29] established a quasi-static model with consideration of thermal effect and proposed a calculation strategy considering the variation of boundary conditions. Using the proposed method, the temperature field and thermal error were predicted accurately. To obtain the key point transient temperatures, Li et al. [30] presented a random thermal network model. Based on the proposed model, the positioning accuracy could be accurately predicted. Beyond that, using a finite element model, Mi et al. [31] study the dynamic characteristics of the spindle nose of a horizontal machining center during the cutting process.

From literature reviews, the physical model-based methods could obtain the vibration response of the system with consideration of different working parameters. The effect of deflect angle has been rarely studied. Due to the incipient fault and periodic maintenance, the working parameters of screw nut such as geometric error and preload can be changed over time. Furthermore, due to the complexity of working condition, the system can be sensitive to the changed parameters. This can lead to the occurrence of unstable vibration and decrease the stability of the system. However, few papers pay attention to the influence of the variation of working parameters on dynamic characteristics of single nut ball screw with five degrees of freedom. The outline of this paper is as follows: Sect. 2 proposes the five-degree-of-freedom nonlinear dynamic model and introduced the relationship between defection angle and contact deformation. Section 3 reveals the effect of excitation amplitude, deflection angle, the number of balls, and preload by the bifurcation diagram and 3-D frequency spectrum. Section 4 measures the dynamic parameters of system and validated the proposed model by vibration response and amplitude frequency curve. Section 5 lists the conclusions.

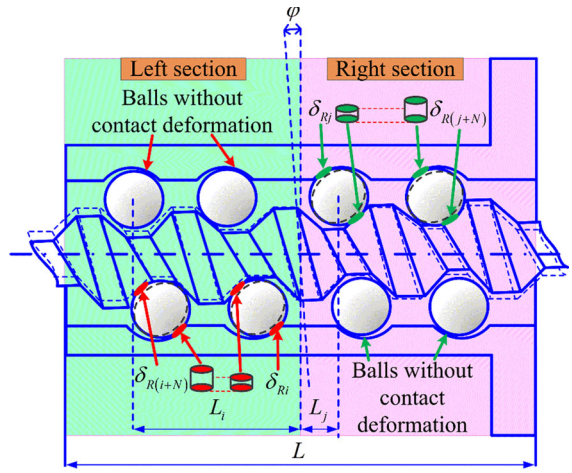

Fig. 1 Schematic of screw nut

2 Dynamic model and governing equations of motion

As shown in Fig. 1, the single nut consists of ball nut, balls, and screw shaft. The single nut is preloaded by variable lead; the value of preload force is given in Table 1. Due to the existence of preload and the difference of contact force, the balls in screw nut can be divided into two parts: left section and right section. Therefore, the axial restoring force of a single nut can be deduced into a piecewise function which can be seen in Eq. 15. In this paper, the feed rate is set to 0. Due to the existence of the initial deflection angle, the deformation of each ball in the screw nut can be different, it depends on the deflection angle φ, the distance L_i and L_j, which is shown in Fig. 1. Therefore, some balls in screw nut can be deformed due to the

Table 1 Parameters for ball screw

Parameters	Value
Pitch circle diameter d_m	42 mm
Lead of ball screw P	16 mm
Ball diameter D	7.144 mm
Initial contact angle α_0	45°
Overall length of screw nut L	144 mm
Number of loaded circles N_c	2.5
Number of loaded balls N	23
Mass of screw shaft m	5.84 kg
Preload F_p [13]	1690 N

unique stress condition, and some balls are not. Because of the nonlinear Hertzian contact force and piecewise restoring function, the vibration system can exhibit a wide variety of dynamics.

According to Ref. [32], the expression of the position angle of ith ball in the left section of ball nut and the position angle of the jth ball in the right section of ball nut can be given by

$$\theta_i = \frac{2\pi}{N}(i-1) \tag{1}$$

$$\theta_j = \frac{2\pi}{N}(j-1) \tag{2}$$

where N is the number of balls per circle in ball nut. As shown in Fig. 1, L_i is the axial distance between ith ball and the center of screw nut in the left section, and L_j is the axial distance between jth ball and the center of screw nut in the right section. The expression of L_i and L_j can be given by

$$L_i = \left(N_c - \frac{\theta_i}{2\pi}\right)P \tag{3}$$

$$L_j = \frac{\theta_j}{2\pi}P \tag{4}$$

P is the lead of screw shaft, and N_c represents the number of loaded circles. According to Refs. [33–35], the elastic deformation along the radial direction of ith ball for the left section of ball nut can be formulated as

$$\delta_{rLi} = \left(x + u_i L_i \varphi_y\right)\cos\theta_i + \left(y - u_i L_i \varphi_x\right)\sin\theta_i \tag{5}$$

and for the right section, the elastic deformation along the radial direction of jth ball of ball nut can be formulated as

$$\delta_{rRj} = \left(x + u_i L_j \varphi_y\right)\cos\theta_j + \left(y - u_i L_j \varphi_x\right)\sin\theta_j \tag{6}$$

where x and y represent the displacement of screw shaft, and φ_x and φ_y are the rocking motions about x- and y-axes Coefficient u_i is a dimensionless constant which can be determined by [33]

$$u_i = \begin{cases} -1 & \text{left section} \\ 1 & \text{right section} \end{cases} \tag{7}$$

The elastic deformation along the axial direction of ith ball for the left section of ball nut can be formulated as [33]

$$\delta_{zLi} = z + \frac{d_m}{2}\left(\varphi_x \sin\theta_i - \varphi_y \cos\theta_i\right) + v_i\left(A\sin\alpha_0 + z_p\right) \tag{8}$$

Similarly, the elastic deformation along the axial direction of jth ball for the right section of ball nut can be formulated as [33]

$$\delta_{zRj} = z + \frac{d_m}{2}\left(\varphi_x \sin\theta_j - \varphi_y \cos\theta_j\right) + v_i\left(A\sin\alpha_0 + z_p\right) \tag{9}$$

where d_{m} represents the pitch circle diameter. The dimensionless constant v_i is dominated on the configuration of rolling elements which can be expressed as follows [33]:

$$v_i = \begin{cases} 1 & \text{left section} \\ -1 & \text{right section} \end{cases} \tag{10}$$

Therefore, the total contact deformation along the contact angle direction of the ball in the left section of screw nut can be formulated as

$$\delta_{Li} = \sqrt{\delta_{rLi}^2 + \delta_{zLi}^2} - A \tag{11}$$

A is the distance between screw shaft raceway curvature center and screw nut raceway curvature center. The total contact deformation along the contact angle direction of the ball in the right section of screw nut can be formulated as

$$\delta_{Rj} = \sqrt{\delta_{rRj}^2 + \delta_{zRj}^2} - A \tag{12}$$

In addition, for the left section of screw nut, the contact angle of the ith ball can be written as

$$\alpha_{Li} = \arctan\left(\delta_{zLi}/\delta_{rLi}\right) \tag{13}$$

and for the right section of screw nut, the contact angle of the jth ball in the right section of screw nut can be written as

$$\alpha_{Rj} = \arctan\left(\delta_{zRj}/\delta_{rRj}\right) \tag{14}$$

According to Refs. [13, 36, 37], the axial piecewise restoring force function can be formulated as

$$F_{NZ}(x,y,z,\varphi_x,\varphi_y,t)=\begin{cases} K\sum_{i=1}^{N}\delta_{iL}^{3/2}\sin\alpha_{Li}-K\sum_{j=1}^{N}\delta_{jR}^{3/2}\sin\alpha_{Rj} & -z_p\le z\le z_p \\ K\sum_{i=1}^{N}\delta_{Li}^{3/2}\sin\alpha_{Li} & z>z_p \\ -K\sum_{j=1}^{N}\delta_{Rj}^{3/2}\sin\alpha_{Rj} & z<-z_p \end{cases} \tag{15}$$

where K is the Hertzian contact stiffness between balls and races, which can be calculated by the method according to Ref. [38]. Furthermore, the restoring force along x- and y-axis can be formulated as

$$F_{Nx}(x,y,z,\varphi_x,\varphi_y,t)=K\sum_{i=1}^{N}\delta_{Li}^{3/2}cos\alpha_{Li}\cos\theta_i+K\sum_{j=1}^{N}\delta_{Rj}^{3/2}cos\alpha_{Rj}\cos\theta_j \tag{16}$$

$$F_{Ny}(x,y,z,\varphi_x,\varphi_y,t)=K\sum_{i=1}^{N}\delta_{Li}^{3/2}\cos\alpha_{Li}\sin\theta_i+K\sum_{j=1}^{N}\delta_{Rj}^{3/2}\cos\alpha_{Rj}\sin\theta_j \tag{17}$$

The restoring moments about x- and y-axis caused by the deformation of balls in screw nut can be expressed as follows:

$$M_{Nx}(x,y,z,\varphi_x,\varphi_y,t)=K\sum_{i=1}^{N}\delta_{Li}^{3/2}\left(\frac{d_m}{2}\sin\alpha_{Li}+L_i\cos\alpha_{Li}\right)\sin\theta_i+K\sum_{j=1}^{N}\delta_{Rj}^{3/2}\left(\frac{d_m}{2}\sin\alpha_{Rj}-L_j\cos\alpha_{Rj}\right)\sin\theta_j \tag{18}$$

$$M_{Ny}(x,y,z,\varphi_x,\varphi_y,t)=K\sum_{i=1}^{N}\delta_{Li}^{3/2}\left(-\frac{d_m}{2}\sin\alpha_{Li}-L_i\cos\alpha_{Li}\right)\cos\theta_i+K\sum_{j=1}^{N}\delta_{Rj}^{3/2}\left(-\frac{d_m}{2}\sin\alpha_{Rj}+L_j\cos\alpha_{Rj}\right)\cos\theta_j \tag{19}$$

Considering the nonlinear contact restoring force and piecewise restoring force, the equivalent dynamic model of screw nut can be simplified as a five-degree-of-freedom mass–spring–damping model which is shown in Fig. 2. According to the analysis of restoring force and restoring moment along x, y, z, φ_x, and φ_y directions, the governing equations of motion for screw nut with five degrees of freedom can be written as follows:

$$m\ddot{x}+c_y\dot{x}+F_{Nx}(x,y,z,\varphi_x,\varphi_y,t)=mg+F_x(t) \tag{20}$$

$$m\ddot{y}+c_y\dot{y}+F_{Ny}(x,y,z,\varphi_x,\varphi_y,t)=F_y(t) \tag{21}$$

$$m\ddot{z}+c_z\dot{z}+F_{NZ}(x,y,z,\varphi_x,\varphi_y,t)=F_z(t) \tag{22}$$

$$I_x\ddot{\varphi}_x+c_y\dot{\varphi}_x+M_{Nx}(x,y,z,\varphi_x,\varphi_y,t)=M_x \tag{23}$$

$$I_y\ddot{\varphi}_y+c_y\dot{\varphi}_y+M_{Ny}(x,y,z,\varphi_x,\varphi_y,t)=M_y \tag{24}$$

where an overdot describes time differentiation; m represents the mass of screw shaft; c_y and c_z represent the viscous damping coefficient along the radial and axial directions. The influence of damping originated from the viscous damping is suitable for the structural characteristics of the proposed model [39]; the value of c_y and c_z can be identified by the test of vibration response, which is shown in Sect. 4. F_x, F_y, and F_z represent the external load. In this study, the expression of external force satisfies $F_x = F_y = F_z = F_0\sin\omega t$, where F_0 is the excitation amplitude and ω represents the excitation frequency. M_x and M_y are the external moment and satisfy $M_x = M_y = lF_0\sin\omega t$, where l is the arm of force and satisfies $l = 0.5L$.

3 Results and discussion

In this section, the numerical solution to the governing equations of the proposed dynamic model is archived by fourth-order Runge–Kutta method. The parameters of the studied ball screw are listed in Table.1. In order to accelerate the convergence of calculation, the initial condition for the differential equations is set to [$\dot{x}$, x, $\dot{y}$, y, $\dot{z}$, z, φ_x, φ_y] = [-3.5741×10^{-4} mm, -3.4863×10^{-4} mm/s, -9.6292×10^{-4} mm, -3.5542×10^{-4} mm/s, -2.0984×10^{-4} mm, -1.0713×10^{-4} mm/s, -3.8483×10^{-4} mm, -8.5445×10^{-4} mm/s, 4.5331×10^{-4} mm, 1.9655×10^{-4} mm/s]; the values are determined by the mean value of the steady-state solution. In this

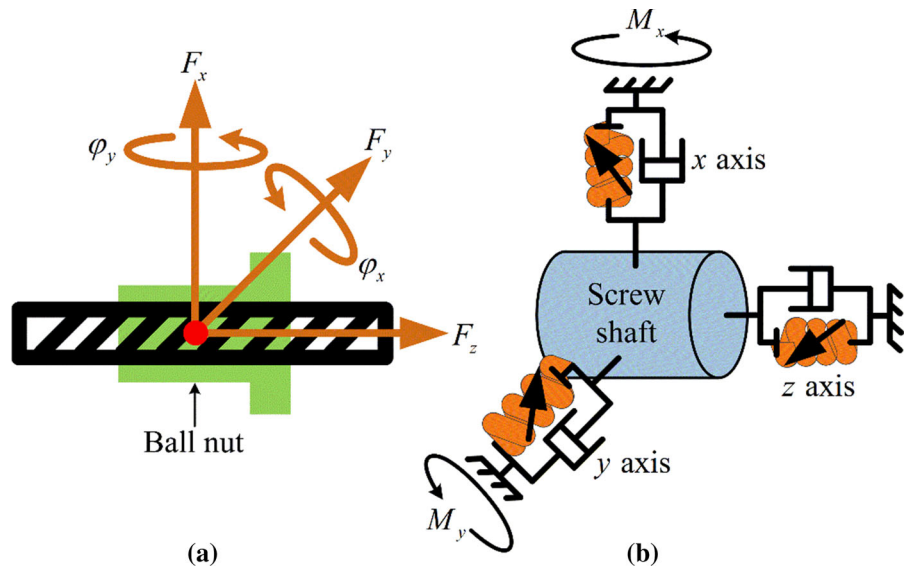

Fig. 2 A lumped spring mass model schematic of ball screw

study, a steady state for a differential equation is a solution where the nature of the motion does not change over time. Considering the time consumption and the required computational accuracy, the time step is set to 5×10^{-6} s, and the absolute tolerance and the relative tolerance are set to 10^{-5}[mm, mm, mm, rad/s, rad/s] and 10^{-5}, respectively. In order to reflect the energy of vibration signal, the root-mean-square value (RMS) is employed to express the amplitude instead of conventional amplitude in amplitude frequency curve (only in Fig. 15). For a vibration response of N values $\{x_1, x_2,\ldots,x_N\}$, the RMS value is [40, 41]

$$\mathrm{RMS} = \sqrt{\frac{1}{N}\left((x_1-\bar{x})^2+(x_2-\bar{x})^2+\cdots+(x_N-\bar{x})^2\right)} \tag{25}$$

where $\bar{x}$ represents the mean value of $\{x_1, x_2,\ldots,x_n\}$. The RMS value is only used in the amplitude frequency curve, the amplitudes are presented in the bifurcation diagram, and 3-D spectrum has a conventional amplitude which can be defined by Poincaré section and fast Fourier transform.

3.1 Effect of excitation amplitude

Excitation amplitude is one of the most significant parameters that influence the dynamic behavior of vibration system. In this subsection, the dynamic behaviors are investigated by bifurcation diagram and 3-D spectrum with excitation amplitude and excitation frequency as control parameters. The waveform, spectrum, phase diagram and Poincaré section are used to analyze the complex dynamic behavior at some specific points.

The corresponding bifurcation diagrams of the vibration system with excitation frequency as control parameter under different excitation amplitude (F_0 = 3000 N, F_0 = 6000 N, F_0 = 9000 N, F_0 = 12000 N, F_0 = 15000 N) are shown in Fig. 3. With the increase in excitation amplitude, the vibration system exhibits a wide variety of dynamic behaviors including chaotic motion, quasiperiodic motion, and period-n motion. In the range of $\omega \in$ [100, 610]rad/s, with the increase in excitation amplitude, more jump discontinuous phenomena appear, and the system exhibits chaotic motion in this interval. In the range of [610, 760]rad/s which is near resonance frequency, the extent of chaotic motion increases markedly, and the chaotic characteristics strengthen. This indicates that the excitation amplitude has impacts on the dynamic behavior of vibration system. Increasing the excitation amplitude, in the range of [960, 1210]rad/s, the influence range of chaotic motion relative to the whole excitation frequency broadens. With a further increase in the excitation frequency, the motion of the system changed from simple period-1 motion to quasiperiodic motion and chaotic motion in the range of [1350, 1730]rad/s.

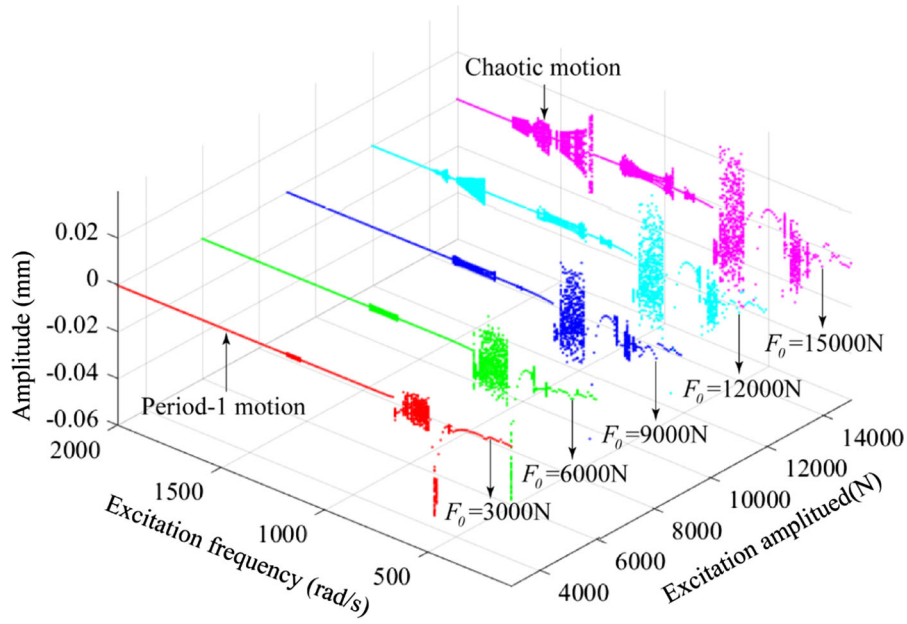

Fig. 3 Bifurcation diagrams with excitation frequency ω as the control parameter at $\varphi = 0°$, $N = 23$, and preload = F_p for different excitation amplitudes F_0

The bifurcation diagram of the system at $F_0 = 15000$ N is exhibited in Fig. 4. The system jumps from one to the other at relatively lower excitation frequency of interval T_1. In the range of T_1, the system exhibits a narrow quasiperiodic motion and chaotic motion. As excitation frequency is increased, the system shows chaotic motion in the range of T_2. Increasing the excitation frequency, the system exhibits period-n and chaotic motion in the interval T_3. By increasing excitation frequency further, after experiencing chaotic motion in the range of T_4, the motion of the system from simple period-1 motion in the interval T_5 enters period-n and quasiperiodic motion in the range of T_6, although at some region the system exhibits chaotic motion, finally to period-1 motion at T_7.

The 3-D frequency spectrum with respect to excitation frequency for different excitation amplitude is illustrated in Fig. 5. At low excitation amplitude, the fundamental frequency f is the dominant frequency component. As the excitation amplitude is increased, the continuous frequency component appears in the

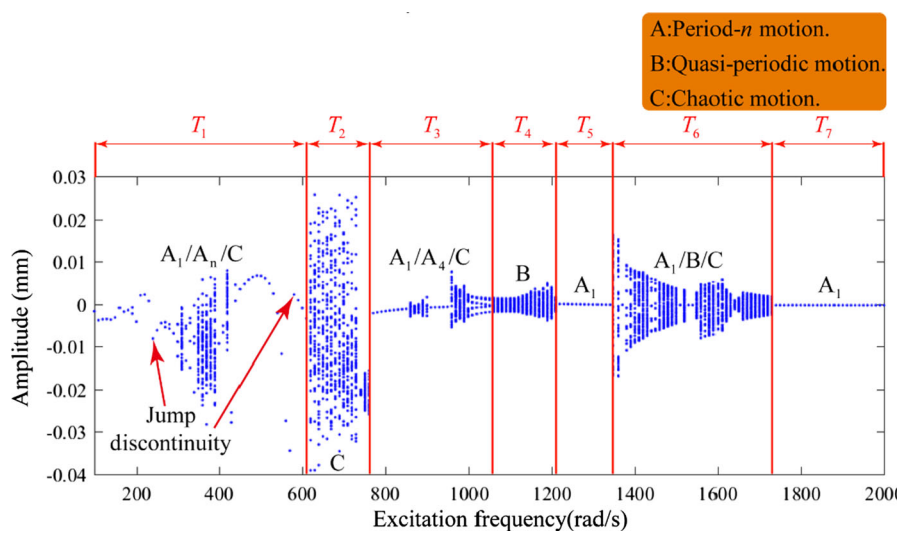

Fig. 4 Bifurcation diagrams with excitation frequency ω as the control parameter at $\varphi = 0°$, $N = 23$, and preload = F_p for $F_0 = 15000$ N

interval [610, 760]rad/s and frequency multiplication (2*f*,3*f*) becomes more obvious. Furthermore, frequency demultiplication (4*f*/5) appears when F_0 = 9000 N, and the main frequency changes from the fundamental frequency *f* to frequency demultiplication (4*f*/5) in the range of [1350, 1700]rad/s when $F_0 > 9000$ N.

To further investigate the effect of excitation amplitude on dynamic behavior of the system, the dynamic response is illustrated with excitation amplitude F_0 as control parameter for different excitation amplitudes in Fig. 6. In Fig. 6a1, the motion of the system exhibits simple period-1 and period-3 motion in interval T_1, and the main frequency is the fundamental frequency *f* in Fig. 6b1. With the increase in excitation amplitude, the system shows quasiperiodic and chaotic motion in the range of T_2, and the vibration

Fig. 6 Dynamic responses of the system with excitation amplitude F_0 as control parameter at $\varphi = 0°$, $N = 23$ and preload = F_p for ω = 360 rad/s, ω = 1000 rad/s and ω = 1460 rad/s. **a** Bifurcation diagram; **b** 3-D frequency spectrum ▶

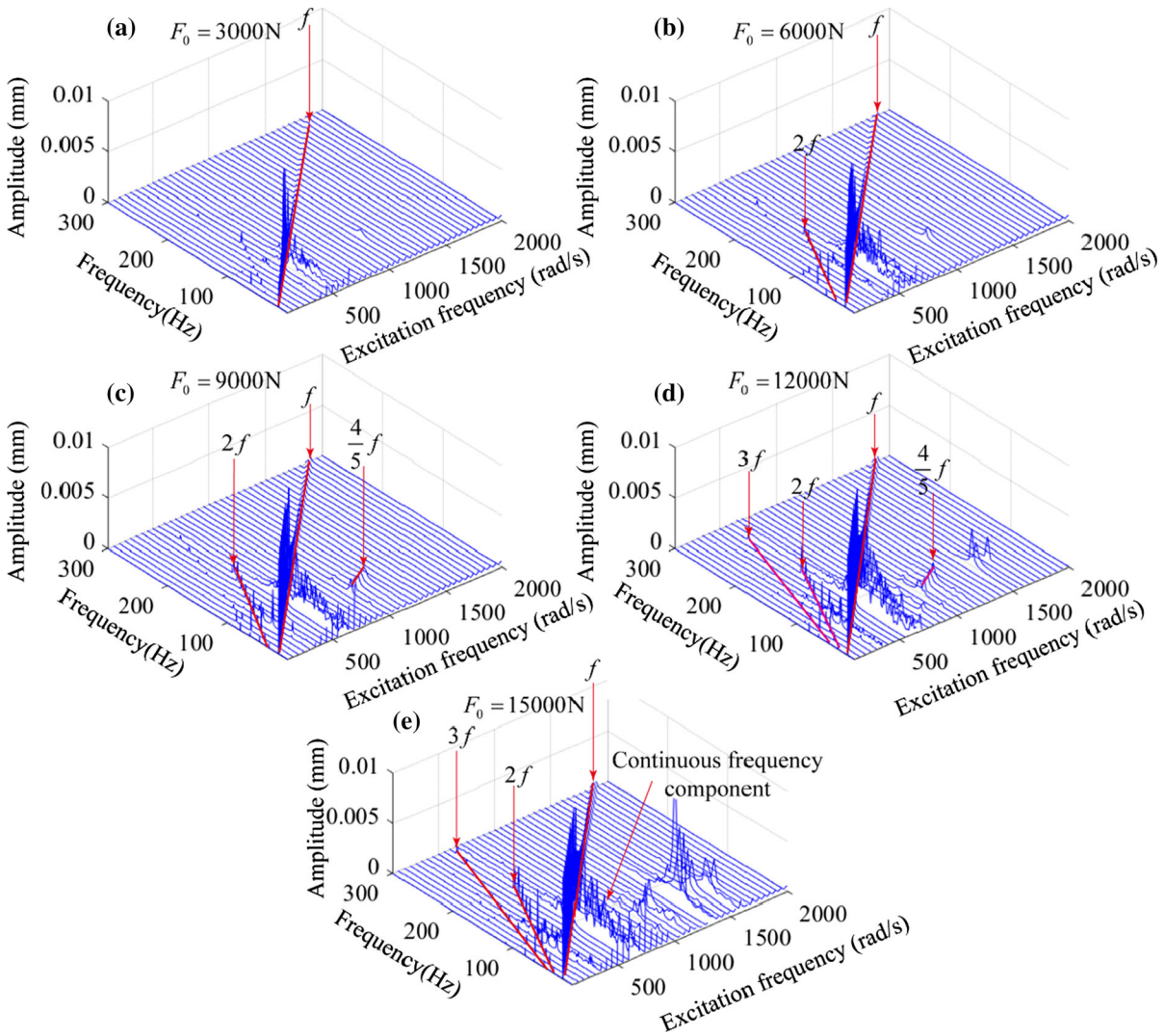

Fig. 5 3-D frequency spectrums for different excitation amplitudes with excitation frequency ω as the control parameter at $\varphi = 0°$, $N = 23$ and preload = F_p for **a** F_0 = 3000 N, **b** F_0 = 6000 N, **c** F_0 = 9000 N, **d** F_0 = 12000 N, **e** F_0 = 15000 N

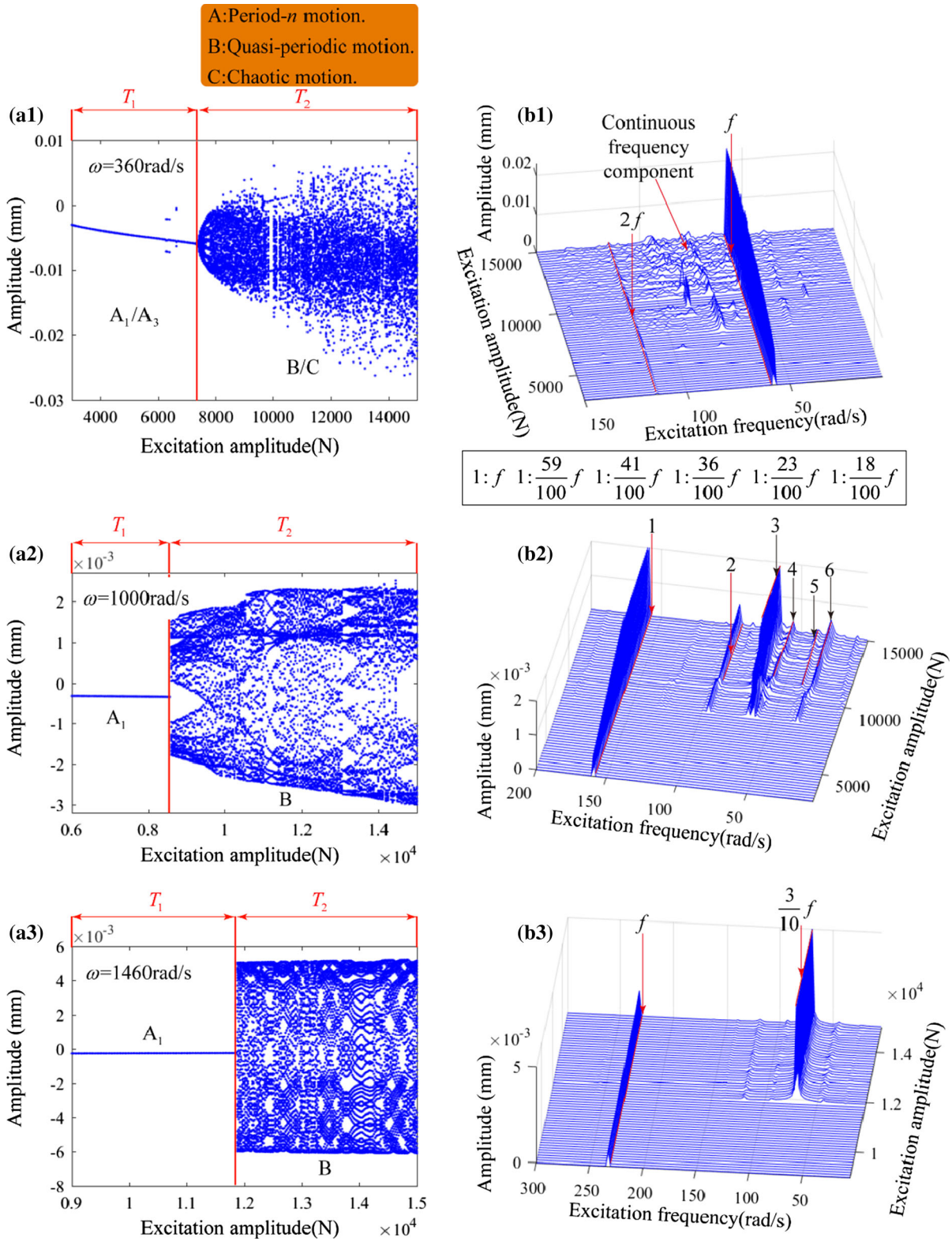
A:Period-n motion.
B:Quasi-periodic motion.
C:Chaotic motion.
(a1)
T1
T2
ω=360rad/s
A1/A3
B/C
Amplitude (mm)
Excitation amplitude(N)
(a2)
ω=1000rad/s
A1
B
×10-3
×10^4
(a3)
ω=1460rad/s
A1
B
(b1)
Continuous frequency component
f
2f
Amplitude (mm)
Excitation amplitude(N)
Excitation frequency(rad/s)
1:f 1:59/100 f 1:41/100 f 1:36/100 f 1:23/100 f 1:18/100 f
(b2)
1
2
3
4
5
6
(b3)
f
3/10 f

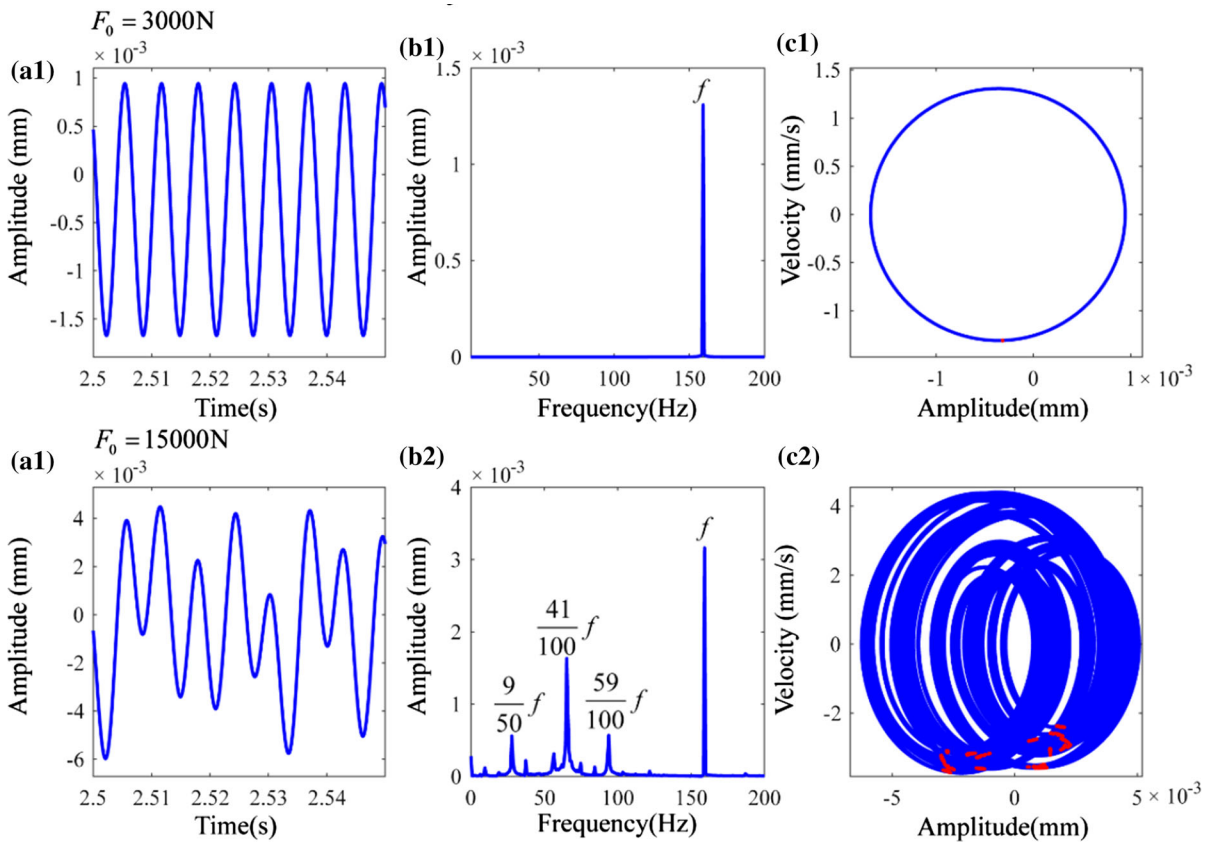

Fig. 7 Vibration responses at $\varphi = 0°$, $N = 23$, $\omega = 1000$ rad/s and Preload = F_p for $F_0 = 3000$ N and $F_0 = 15000$ N. **a** Waveform, **b** frequency, **c** phase diagram and Poincaré section

system shows continuous frequency component. As shown in Fig. 6a2 and a3, the system exhibits simple period-1 motion at T_1 and quasiperiodic motion in interval T_2. Beyond that, as shown in Fig. 6b3, $3f/10$ becomes the main frequency as an excitation amplitude is $F_0 > 8600$ N.

Figure 7 shows the corresponding vibration response at $F_0 = 3000$ N and $F_0 = 15000$ N when $\omega = 1000$ rad/s. In Fig. 7c1, the Poincaré section shows only one point and the phase diagram shows a closed circle, which further proves that the system exhibits a simple period-1 motion. In Fig. 7c2, there exist finite points in the Poincaré section and the phase diagram is regular, where the system exhibits quasiperiodic motion. The comparison of vibration response between $F_0 = 9000$ N and $F_0 = 15000$ N at $\omega = 1460$ rad/s is shown in Fig. 8, where the system presents quasiperiodic motion at $F_0 = 15000$ N. However, the 2-frequency quasiperiodic motions are rare and interesting observations in mechanical system. The similar phenomena in machine tool vibrations can be observed in Ref. [42] and Ref. [43]. Figure 9 shows the comparison between $F_0 = 12000$ N and $F_0 = 15000$ N at $\omega = 1590$ rad/s. When $F_0 = 15000$ N, the waveform loses the periodicity in Fig. 9a2, and the continuous spectral appears in Fig. 9b2. As can be seen in Fig. 9c2, there exists infinite point in the Poincaré section, and the phase diagram is irregular and loses periodicity, which illustrates that the system presents chaotic motion at this point.

Therefore, at relative low excitation amplitude, the vibration system exhibits less nonlinear dynamic properties. In addition, except the region near resonance frequency, the motion of the system exhibits simple period-1 motion. When the excitation amplitude becomes higher, the system presents a wide variety of dynamic behaviors. These further proved that the excitation amplitude has a considerable impact on the dynamic characteristic of the system.

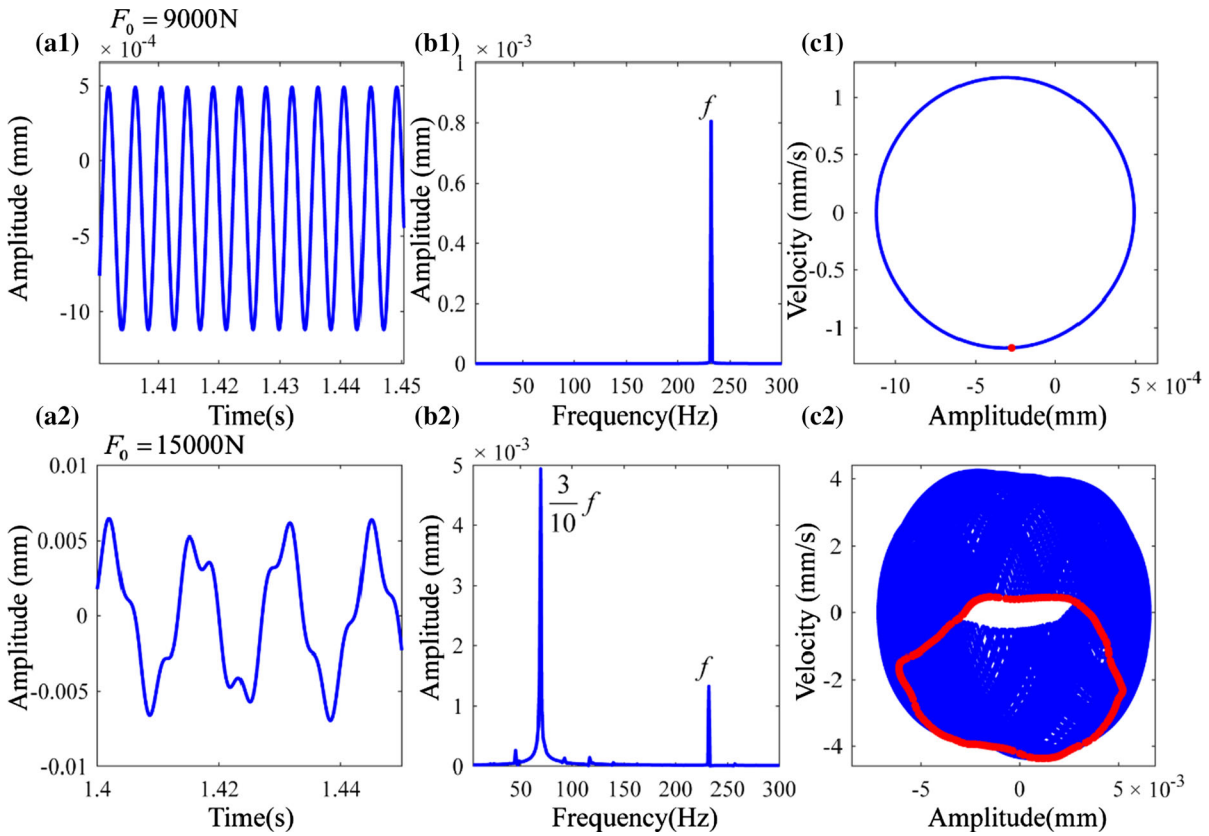

Fig. 8 Vibration responses at $\varphi = 0°$, $N = 23$, and $\omega = 1460$ rad/s and Preload = F_p for $F_0 = 9000$ N and $F_0 = 15000$ N. **a** Waveform, **b** frequency, **c** phase diagram and Poincaré section

3.2 Effect of deflection angle

In the previous studies, the deflection angle of ball screw is often ignored. However, due to human error and assembly error the deflection angle is inevitable to some extent. Considering the complex working conditions, the investigation of defection angle on nonlinear dynamic characteristics is crucial. In this subsection, the nonlinear dynamics of the system with deflection angle and excitation frequency as control parameter are examined.

The comparison of dynamic response between $\varphi = 0°$ and $\varphi = 0.5°$ is shown in Fig. 10. As shown in Fig. 10a1, the vibration system exhibits simple period-1 motion in the interval T_1, and in Fig. 10b1 the main frequency is the fundamental frequency f. As the excitation frequency is increased, the system exhibits quasiperiodic motion in the range of T_2, and frequency demultiplication ($f/5$, $2f/5$, $3f/5$) is shown in Fig. 10b1. Increasing the deflection angle from 0° to 0.5°, the nonlinear characteristics strengthen. As seen in Fig. 10a2, the system shows period-1 motion in the range of T_1, experiencing period-1 and period-5 motion in the range of T_2, to quasiperiodic motion in the interval T_3. It can be seen in Fig. 10b2 that the fundamental frequency is the dominant frequency component, and the frequency demultiplication ($f/5$, $2f/5$, $3f/5$, $4f/5$) is lower than f. With the increase in excitation amplitude, the motion of system enters quasiperiodic motion in the interval [1047, 1090]rad/s. Furthermore, no complicated chaotic motion appears.

In order to further study the effect of deflection angle on dynamic response, Figure 11 shows the corresponding bifurcation diagram and 3-D frequency spectrum with deflection angle as control parameter at $\omega = 1008$ rad/s and $\omega = 1050$ rad/s. It can be seen in Fig. 11a1 and b1, after experiencing a short period-1 motion at relatively small deflection, the system enters quasiperiodic motion in the interval T_1, the main frequency is demultiplication frequency $3f/5$, and the

fundamental frequency f is the second largest. Increasing the deflection angle, the motion of the system presents period-1 motion again in the range of T_2, and the fundamental frequency f becomes the largest frequency component. By increasing the deflection angle further, the system enters quasiperiodic motion, and demultiplication frequency $3f/5$ becomes the dominant frequency in the interval T_3. Similarly, as shown in Fig. 11a2, the system exhibits simple period-1 motion in the interval T_1, and the system presents two types of motion state at T_2, i.e., period-1 motion and period-5 motion. Moreover, the fundamental frequency f is the dominant frequency component and the demultiplication frequency component $2f/5$ is the second largest which is shown in Fig. 11b2. The comparison of vibration response between $\varphi = 0°$ and $\varphi = 0.02°$ at $\omega = 1050$ rad/s is shown in Fig. 12. As seen in the figure, with the increase in deflection angle, the motion of the system changed from simple period-1 motion to quasiperiodic motion. Moreover, the comparison of vibration response between $\varphi = 0°$ and $\varphi = 0.5°$ at $\omega = 1008$ rad/s is shown in Fig. 13 which indicates that the increase in deflection leads the motion of the system to change from period-1 motion to quasiperiodic motion.

Fig. 10 Dynamic responses of the system with excitation frequency ω as control parameter at $F_0 = 6000$ N, $N = 23$ and preload = F_p for $\varphi = 0°$ and $\varphi = 0.5°$. **a** Bifurcation diagram; **b** 3-D frequency spectrum

3.3 Effect of the number of balls

The number of balls is closely corresponding to the required rigid and the lead of screw shaft and then significantly changes the dynamic characteristics of

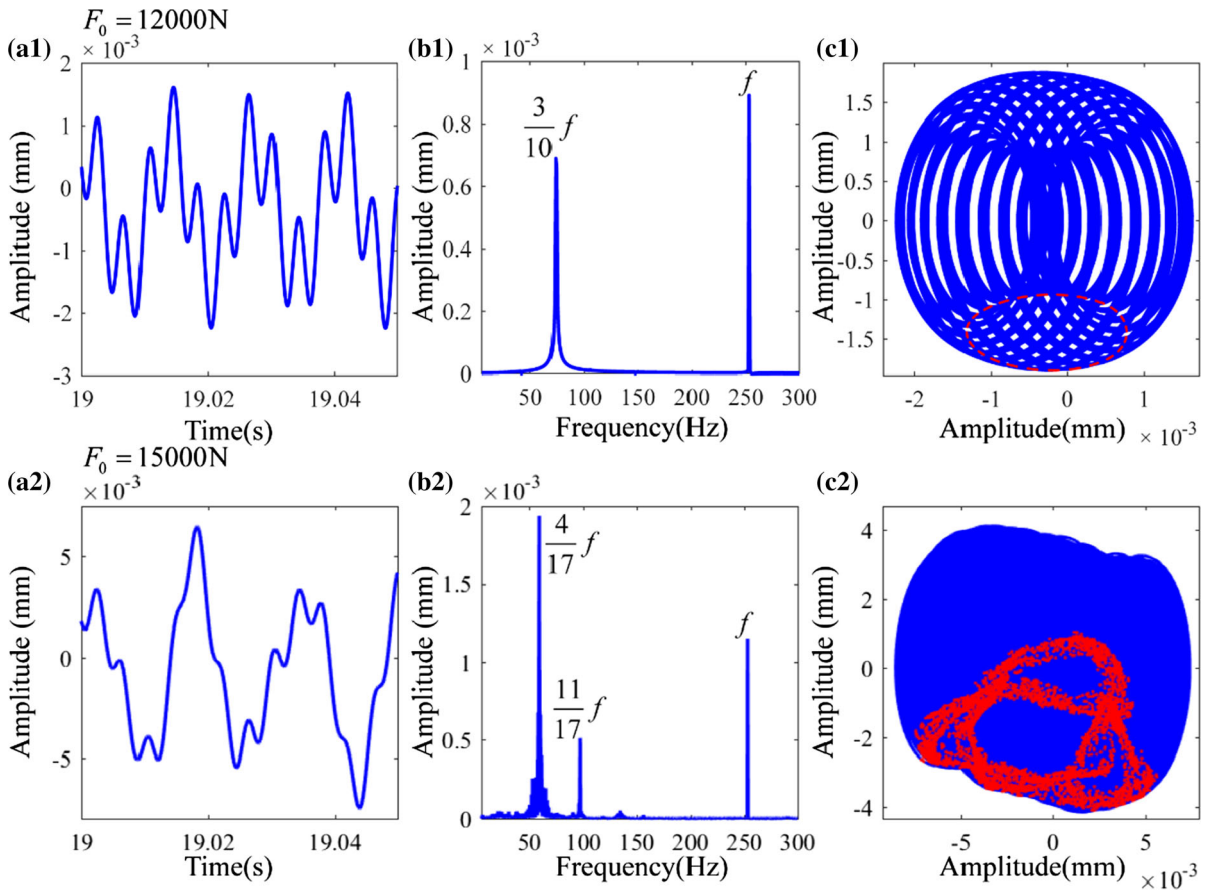

Fig. 9 Vibration responses at $\varphi = 0°$, $N = 23$, $\omega = 1590$ rad/s and Preload = F_p for $F_0 = 12000$ N and $F_0 = 15000$ N. **a** Waveform, **b** frequency, **c** phase diagram and Poincaré section

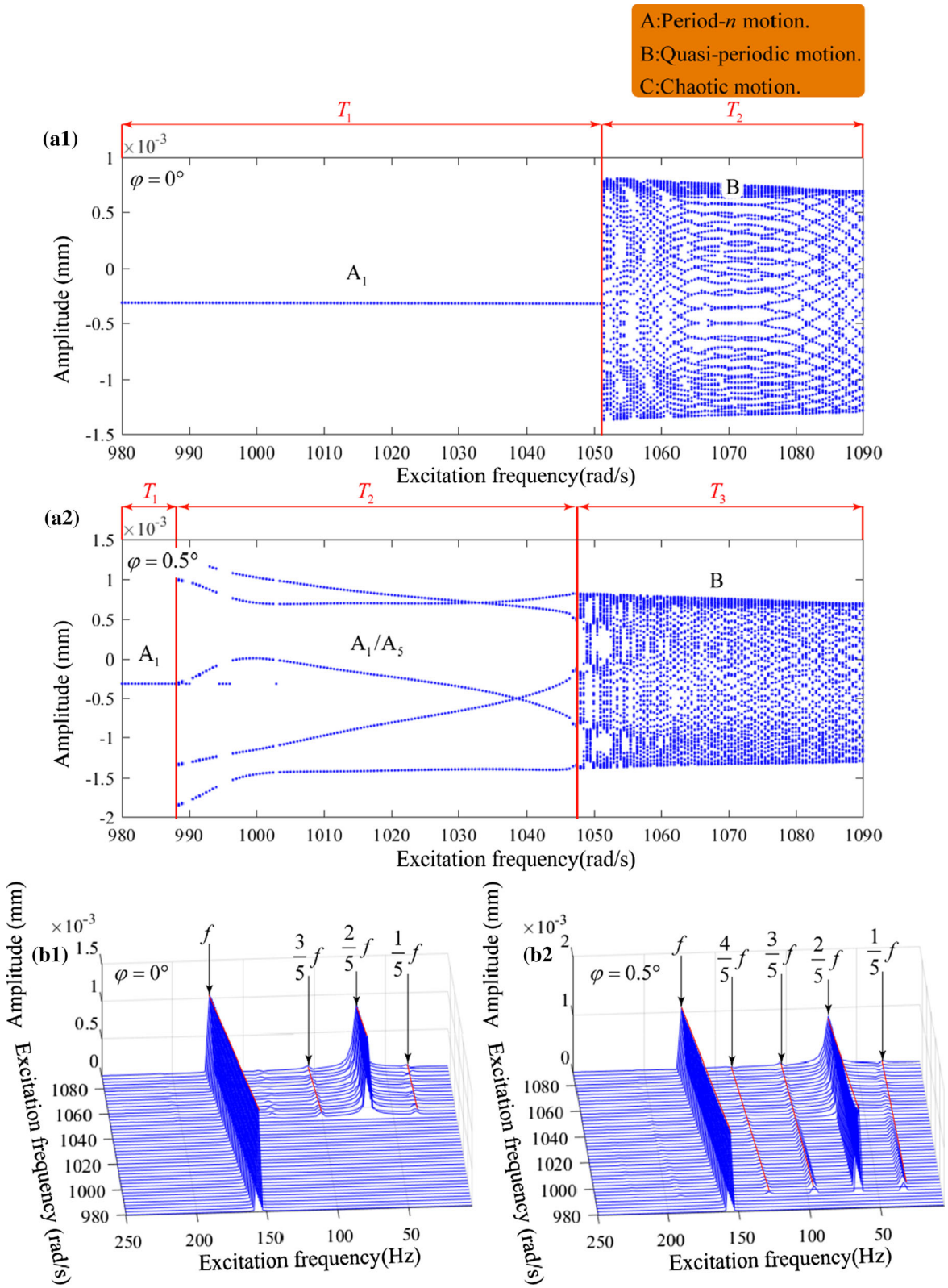
A:Period-n motion.
B:Quasi-periodic motion.
C:Chaotic motion.
(a1)
T_1
T_2
$\times 10^{-3}$
$\varphi = 0°$
A1
B
Amplitude (mm)
Excitation frequency(rad/s)
(a2)
T_1
T_2
T_3
$\varphi = 0.5°$
A1
A1/A5
B
(b1)
$\varphi = 0°$
(b2)
$\varphi = 0.5°$
f
$\frac{3}{5}f$
$\frac{2}{5}f$
$\frac{1}{5}f$
$\frac{4}{5}f$
Excitation frequency (rad/s)
Excitation frequency(Hz)

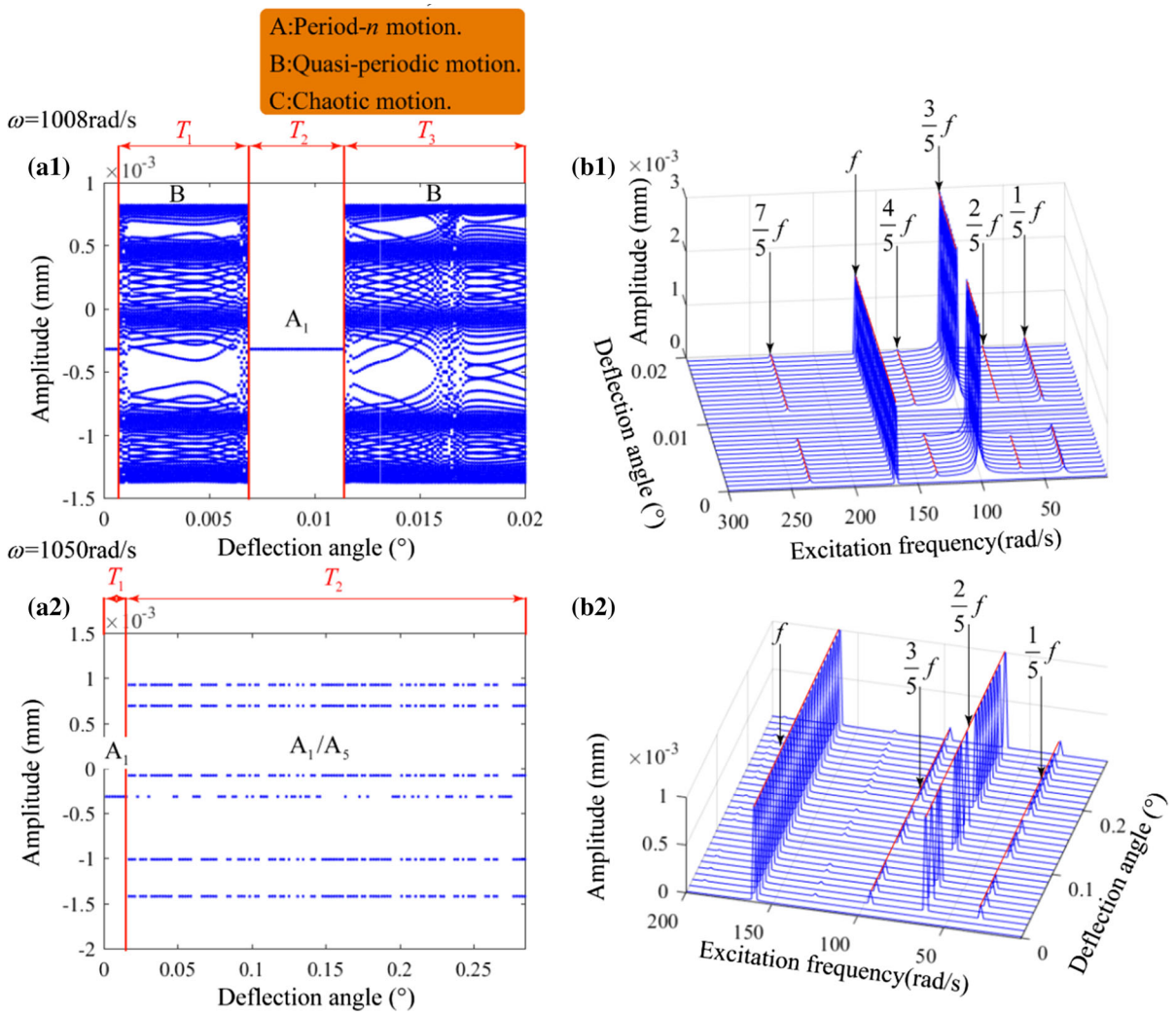

Fig. 11 Dynamic responses of the system with deflection angle φ as control parameter at F_0 = 6000 N, N = 23 and Preload = F_p for ω = 1008 rad/s and ω = 1050 rad/s. **a** Bifurcation diagram; **b** 3-D frequency spectrum

ball screw. Because the range of working frequency is fixed, it is important to determine a suitable number to guarantee the dynamic performance of the system. In this subsection, the dynamic responses are exhibited with respect to excitation frequency. To further study the effect of the number of balls on the dynamic characteristic, the bifurcation diagrams with different numbers of balls (N = 10, N = 23, N = 36) are shown in Fig. 14. It can be seen in the figure that chaotic motion, quasiperiodic motion, and period-n motion can make a distinction between each other, and the critical transformation frequency among different kinds of motions can be identified. As the decrease in the number of balls, all three cases present chaotic motion near the resonance frequency, and the corresponding resonance frequency is reduced. Moreover, at the excitation frequency which is lower than resonance frequency, jump discontinuous phenomena can be observed repeatedly.

Depending on the variation of stiffness caused by different numbers of balls, the resonance frequency increases with the number of balls. As shown in Fig. 15, the resonance frequency and sub-harmonic resonance frequency increase, and the peak value of amplitude frequency curves enhances. In order to further illustrate the influence of the number of balls, Fig. 16 presents the corresponding bifurcation diagrams at relative low excitation frequency $\omega \in$ [100,

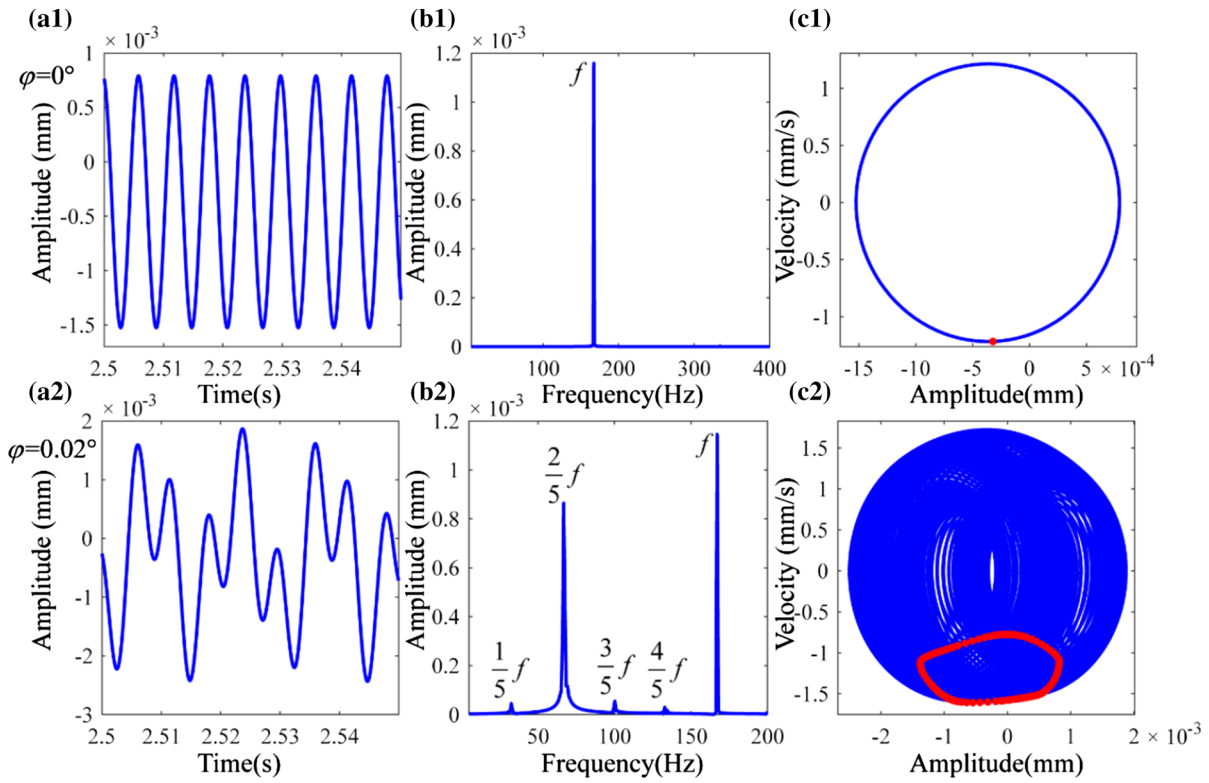

Fig. 12 Vibration responses at $N = 23$, $F_0 = 6000$ N $\omega = 1050$ rad/s and preload = F_p for $\varphi = 0°$ and $\varphi = 0.02°$. **a** Waveform, **b** frequency, **c** phase diagram and Poincaré section

500]rad/s. In Fig. 16a, in the interval T_1, the response repeatedly shows jump discontinuous phenomenon, and the system exhibits period-1 and period-2 motion. Increasing the excitation frequency further, the system exhibits period-n and chaotic motion in the range of T_2. As seen in Fig. 16b, when the number of balls decreases from $N = 36$ to $N = 10$, the system exhibits a wide variety of dynamic behaviors in the range of $\omega \in [100, 500]$rad/s. In the interval T_1, the motion of the system is period-1. As the increase in excitation frequency, different motion states can be observed, such as period-n, quasiperiodic, and chaotic motion in the range of T_2. After experiencing chaotic motion in interval T_3, the motion of the system enters period-1 and chaotic motion in the range of T_4. The corresponding 3-D frequency spectrums are shown in Fig. 17, and the continuous frequency components can be distinguished from other discrete frequency components, as shown in Fig. 17b.

3.4 Effect of preload

By creating a load between screw shaft and ball nut, a preload can bring greater stiffness to ball screw. Therefore, the displacement of structure can be reduced when the system is under external force. In this subsection, to investigate the influence of preload on the dynamic behaviors, the preload F_p and excitation frequency ω are chosen as control parameter. The corresponding 3-D bifurcation diagrams with respect to excitation frequency are shown in Fig. 18; five different values of the preload, i.e., preload = F_p, preload = $1.2F_p$, preload = $1.4F_p$, preload = $1.6F_p$, and preload = $1.8F_p$, are studied. With the decrease in preload, the system exhibits different kinds of motion states. The system only exhibits simple period-1 motion and quasiperiodic motion when the preload $\geq 1.6F_p$, and the main frequency in Fig. 19d and e is the fundamental frequency f. Decreasing the preload from $1.4F_p$ to $1.2F_p$, as shown in Fig. 18, the interval of quasiperiodic and chaotic motion relative to the whole excitation frequency broadens, and

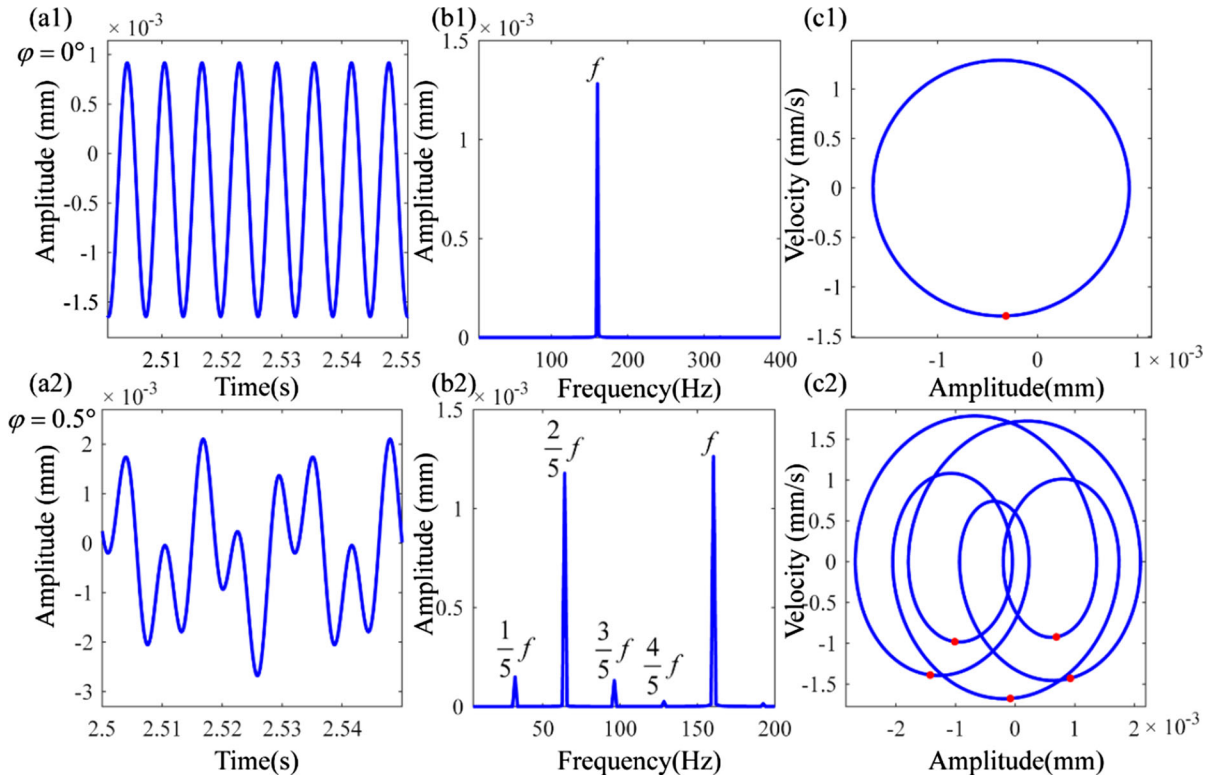

Fig. 13 Vibration responses at $N = 23$, $F_0 = 6000$ N $\omega = 1008$ rad/s and preload = F_p for $\varphi = 0°$ and $\varphi = 0.5°$. **a** Waveform, **b** frequency, **c** phase diagram and Poincaré section

frequency demultiplication (4*f*/13) appears as shown in Fig. 19b and c. By further decreasing the preload from $1.2F_p$ to F_p, the region of period-*n*, quasiperiodic, and chaotic motion continuously broadens, and continuous spectrum appears as shown in Fig. 19a. This indicates that lower preload can degrade the dynamic performance of ball screw in some specific excitation frequency range.

As shown in Fig. 20, in order to further investigate the influence of preload, the dynamic response at $\omega = 1585$ rad/s and $\omega = 1585$ rad/s is exhibited with preload as control parameter. It can be seen from Fig. 20a1 and Fig. 20b1 that the system exhibits chaotic motion in the range of T_1. The corresponding 3-D frequency spectrum shows that the fundamental frequency component f is the second largest, and continuous frequency component appears in the interval T_1. As the increase in preload, the system enters quasiperiodic motion in the range of T_2, except at some points where the motion of the system is period-1, the continuous frequency component disappeared, and 3*f*/10 becomes the dominant frequency component. Increasing the preload further, the system presents simple period-1 motion in the range of T_3, and the main frequency in 3-D spectrum is the fundamental frequency f. Similarly in Fig. 20a2 and b2, after experiencing quasiperiodic motion in the range of T_1, the system enters period-1 motion in the interval T_2, and the main frequency changed from frequency demultiplication (6*f*/25 and 7*f*/25) in the range of T_1 to fundamental frequency f in the range of T_2. The dynamic behavior of quasiperiodic motion at $\omega = 1680$ rad/s and preload = F_p is exhibited in Fig. 21, which presents that the system exhibits quasiperiodic motion at this point.

4 Experimental verification

To validate the proposed dynamic model and obtain the dynamic parameters used in the previous section, an experiment is set up in this section. The top view schematic of experiment setup is shown in Fig. 22. As seen in the figure, the ball screw (THK SBN4016) is

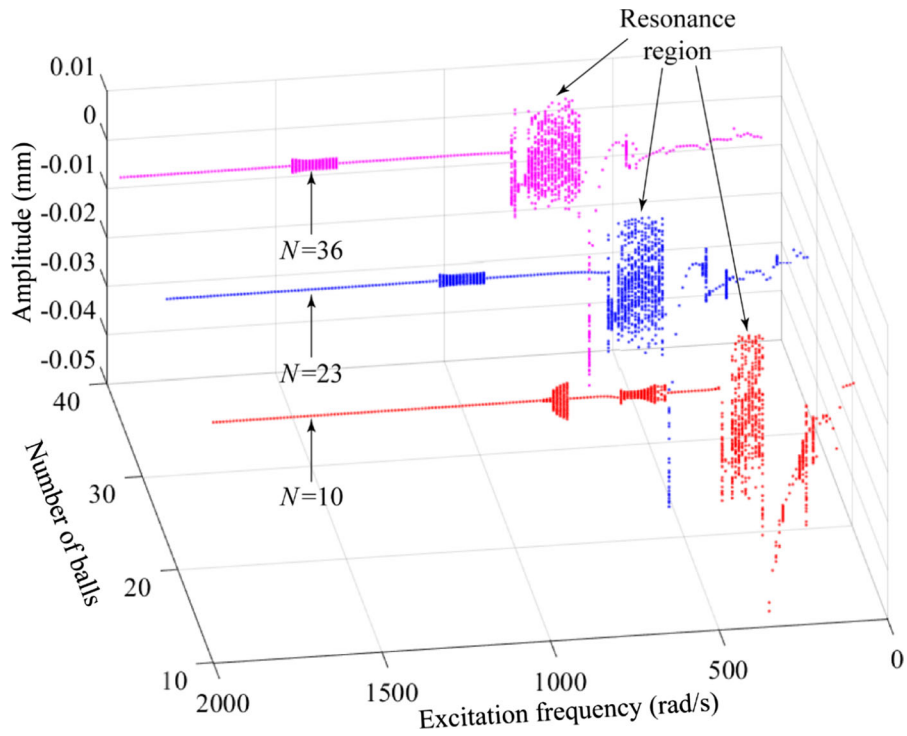

Fig. 14 Bifurcation diagrams with excitation frequency ω as the control parameter at, F_0 = 6000 N, φ = 0°, and preload = F_p for N = 10, N = 23 and N = 36

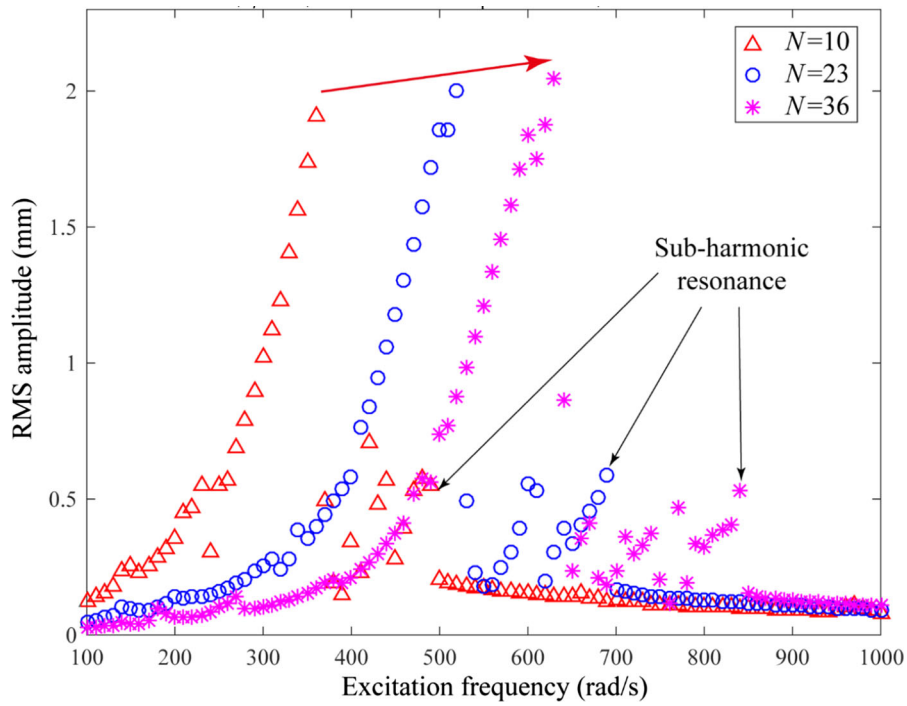

Fig. 15 Amplitude frequency curve at N = 23, F_0 = 6000 N, φ = 0°, and preload = F_p for the number of balls N = 10, N = 23 and N = 36

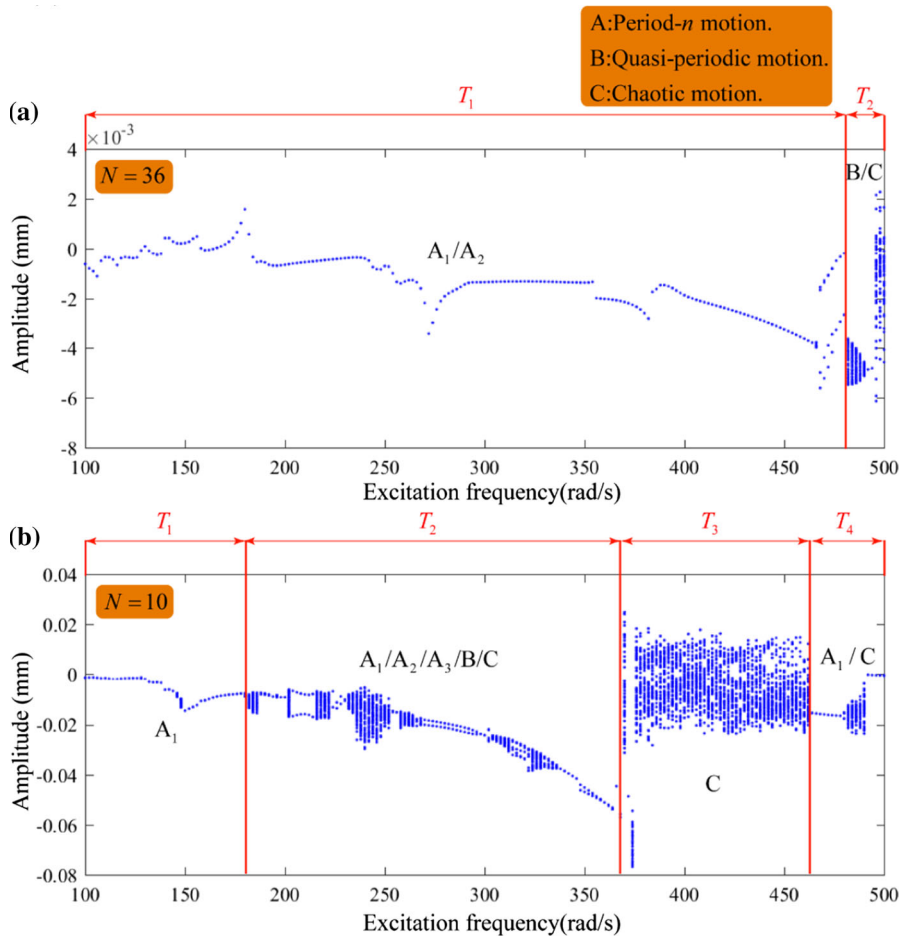

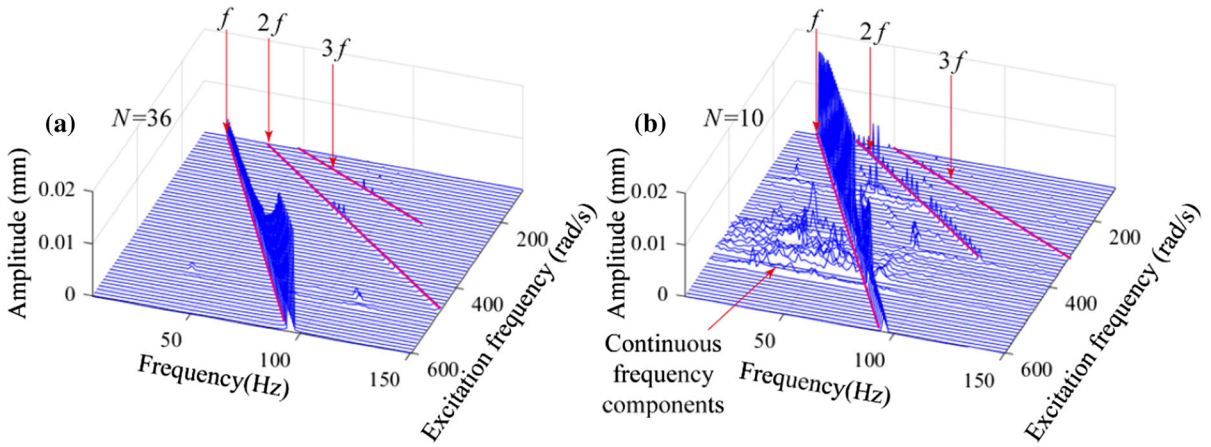

Fig. 16 Bifurcation diagrams with excitation frequency ω as the control parameter at $\varphi = 0°$, $F_0 = 6000$ N, and preload = F_p for different numbers of balls. **a** $N = 36$, **b** $N = 10$

Fig. 17 3-D frequency spectrums with excitation frequency ω as the control parameter at $\varphi = 0°$, $F_0 = 6000$ N, and preload = F_p for different numbers of balls. **a** $N = 36$, **b** $N = 10$

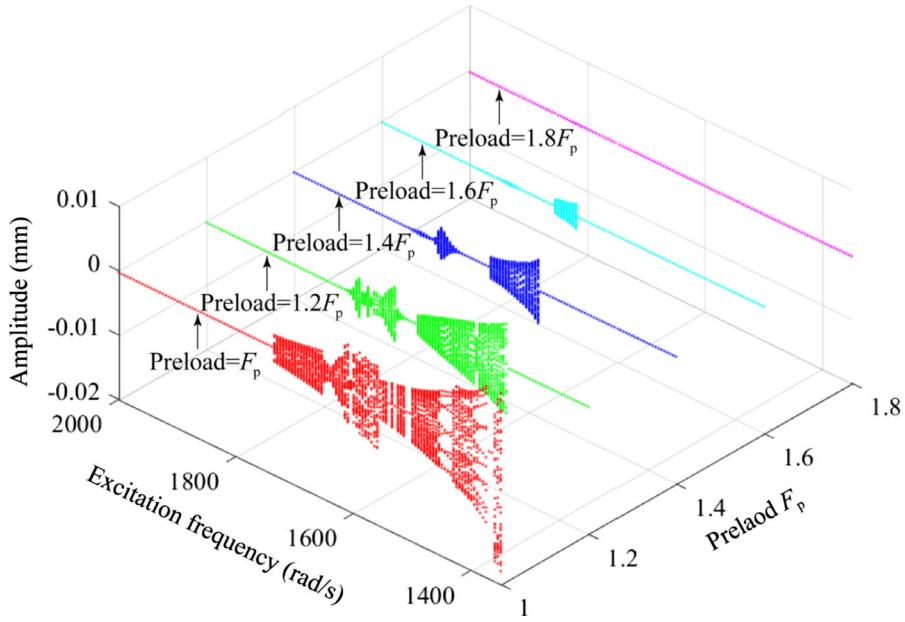

Fig. 18 Bifurcation diagrams with excitation frequency ω as the control parameter at $N = 23$, $F_0 = 15000$ N and $\varphi = 0°$ for different preload. **a** Preload = F_p, **b** preload = $1.2F_p$, **c** preload = $1.4F_p$, **d** preload = $1.6F_p$, **e** preload = $1.8F_p$

fixed on a test rig. The parameters of ball screw are listed in Table 1. In the experiment, the deflection angle of screw shaft is generated by a hydraulic jack acting on the right end of screw shaft, and the dial gauge is used to measure the static displacement in the circumferential direction. The vibration response is measured by the accelerometer (Sinocera CA-YD-189) mounted on the right end of screw shaft. Using an electromagnetic shaker (Sinocera JZK-50) to generate harmonic excitation, a piezoelectric force senor (Sinocera CL-YD-331A) is used to measure the excitation amplitude acting on screw shaft along z-axis. As shown in the figure, the signal collection and generating system consist of a power amplifier (YE5874A), a signal generator (Sinocera YE1311), a charge amplifier (Sinocera YE5874A), a data collection system (DH5956), and a PC.

In this study, the half-power bandwidth method is employed to extract damping ratios from the frequency response function. The frequency response function along y and z directions can be obtained by impact test, and the result is shown in Fig. 23. According to the equation in Ref. [44], the expression of damping ratio ζ can be given by

$$\zeta = \frac{\omega_2 - \omega_1}{2\omega_{dm}} \tag{26}$$

where ω_{dm} represents the nature frequency of screw nut, ω_1 and ω_2 are the half-power frequency when the corresponding amplitude $A = 0.707A_{\max}$, where $A_{\max}$ represents the corresponding amplitude of ω_{dm}. Therefore, the results are shown in Fig. 23, $\omega_{y1} = 65.3$ Hz, $\omega_{y2} = 66.935$ Hz, $\omega_{ydm} = 65.9$ Hz, $\omega_{z1} = 96.85$ Hz, $\omega_{z2} = 101.2$ Hz, $\omega_{zdm} = 102$ Hz. Based on the measurement results above, the dimensionless damping ratio along y-axis $\zeta y = 0.0124$ and z-axis $\zeta z = 0.0213$ can be estimated. The viscous damping coefficient c used in the previous section can be calculated by $c = 4\pi\zeta\omega_0 m$; hence, the value of c_y and c_z can be evaluated. Furthermore, the amplitude frequency curve of screw nut from simulation and experiment is compared in Fig. 24. The difference of the nature frequency from experiment and simulation is 1.6%, which validates the proposed model. In order to verify the proposed method with the consideration of deflection angle, two values of excitation frequency, i.e., $\omega/2\pi = 74$ Hz and $\omega/2\pi = 126$ Hz, are selected to compare the vibration response between experiment and simulation, which is seen in Fig. 25. According to the measuring result of dial gauge, the deflection angle equals 0.7162°. The comparison of vibration response between the selected two points is shown in Fig. 25.

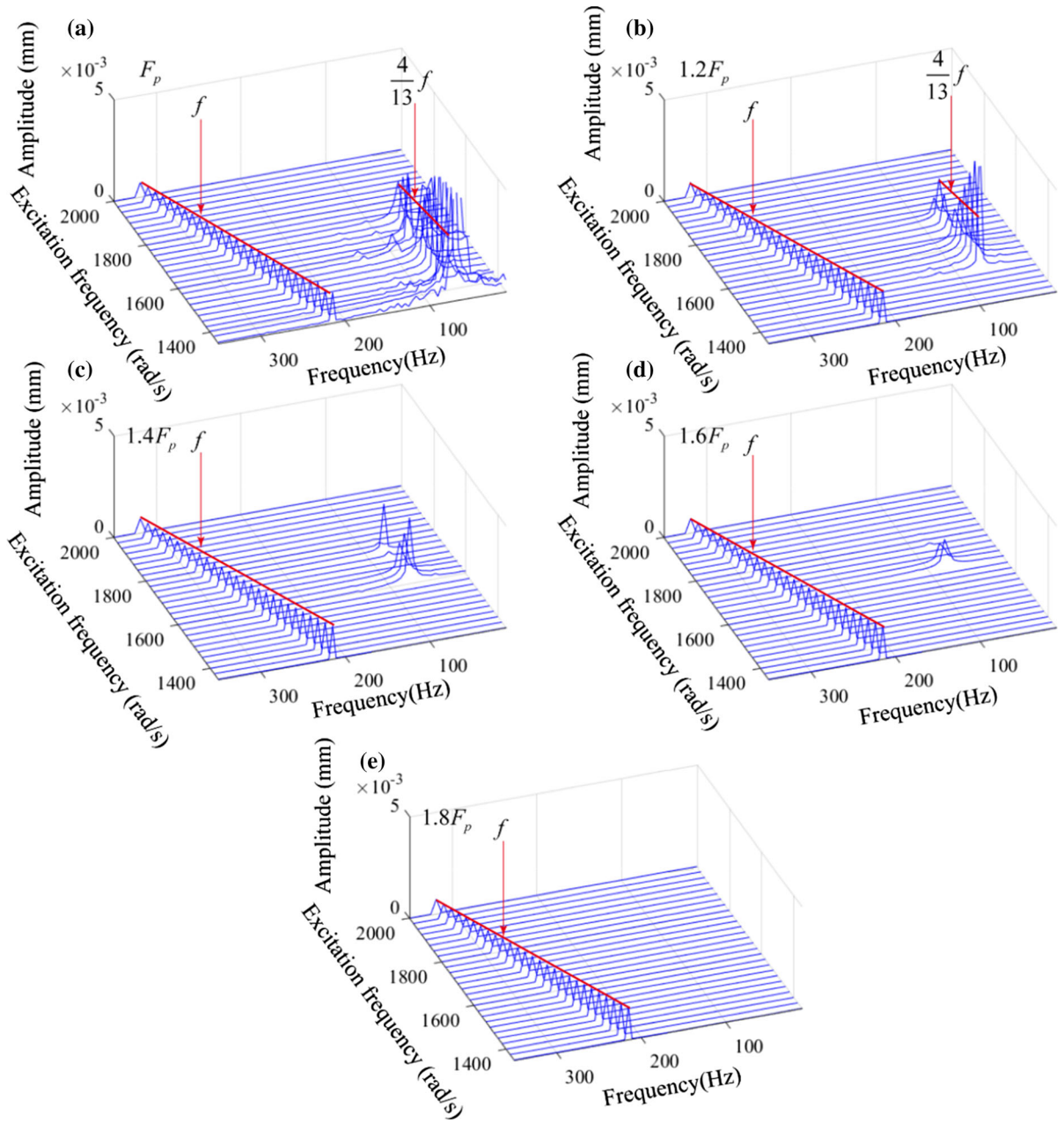

Fig. 19 3-D frequency spectrum with excitation frequency ω as control parameter at $N = 23$, $F_0 = 15000$ N and $\varphi = 0°$ for different preload. **a** Preload = F_p, **b** preload = $1.2F_p$, **c** preload = $1.4F_p$, **d** preload = $1.6F_p$, **e** preload = $1.8F_p$

5 Conclusion

In this paper, a five-degree-of-freedom dynamic model of variable lead preloaded single nut ball screw considering the effect of deflection angle is proposed; the proposed model is investigated by the numerical method. The relationship between the deflection angle and the contact deformation of each ball is given. The effects of different system parameters, i.e., excitation

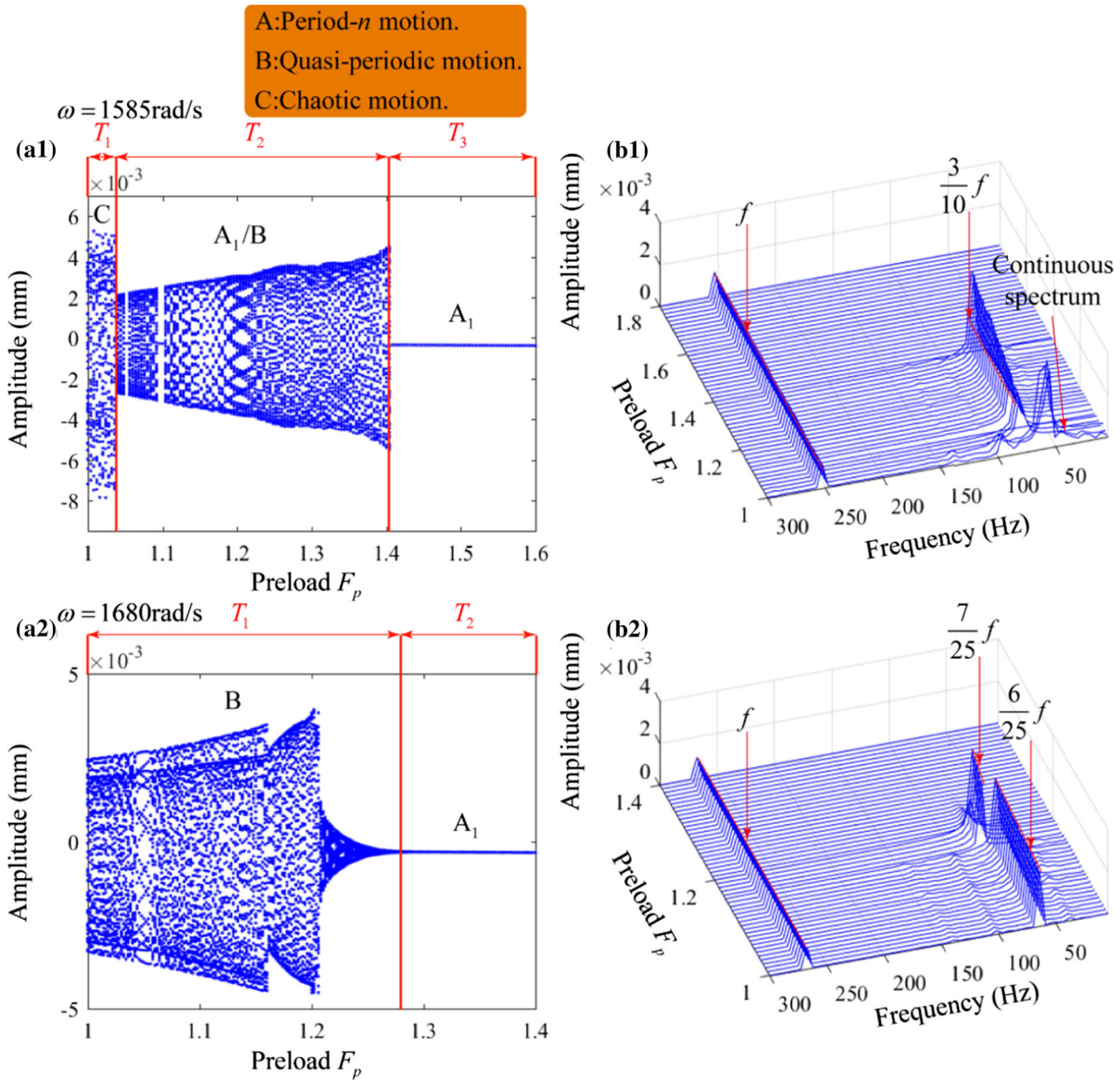

Fig. 20 Dynamic responses of the system with deflection angle preload as control parameter at F_0 = 15000 N, and N = 23 for ω = 1585 rad/s, and ω = 1680 rad/s. **a** Bifurcation diagram; **b** 3-D frequency spectrum

amplitude, deflection angle, the number of balls, and preload, are quantitatively studied. Bifurcation diagram, 3-D frequency spectrum, and RMS value amplitude frequency curves with respect to different parameters are used to study the influence on dynamic behaviors. To validate the proposed dynamic model and estimate the dynamic parameters, a series of experiments are conducted. The main conclusions of this study are listed as follows:

(1) Based on different system parameters, the system presents various nonlinear dynamics, namely period-n motion, quasiperiodic motion, chaotic motion, and jump discontinuity phenomenon.

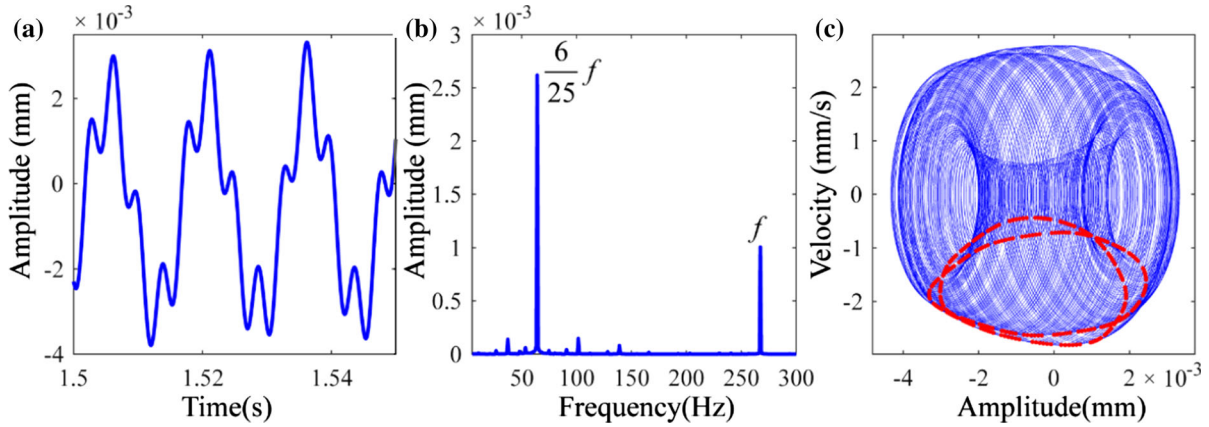

Fig. 21 Vibration responses at preload = F_p, $N = 23$, $F_0 = 15000$ N and $\varphi = 0°$ for $\omega = 1680$ rad/s. **a** Waveform, **b** frequency, **c** phase diagram and Poincaré section

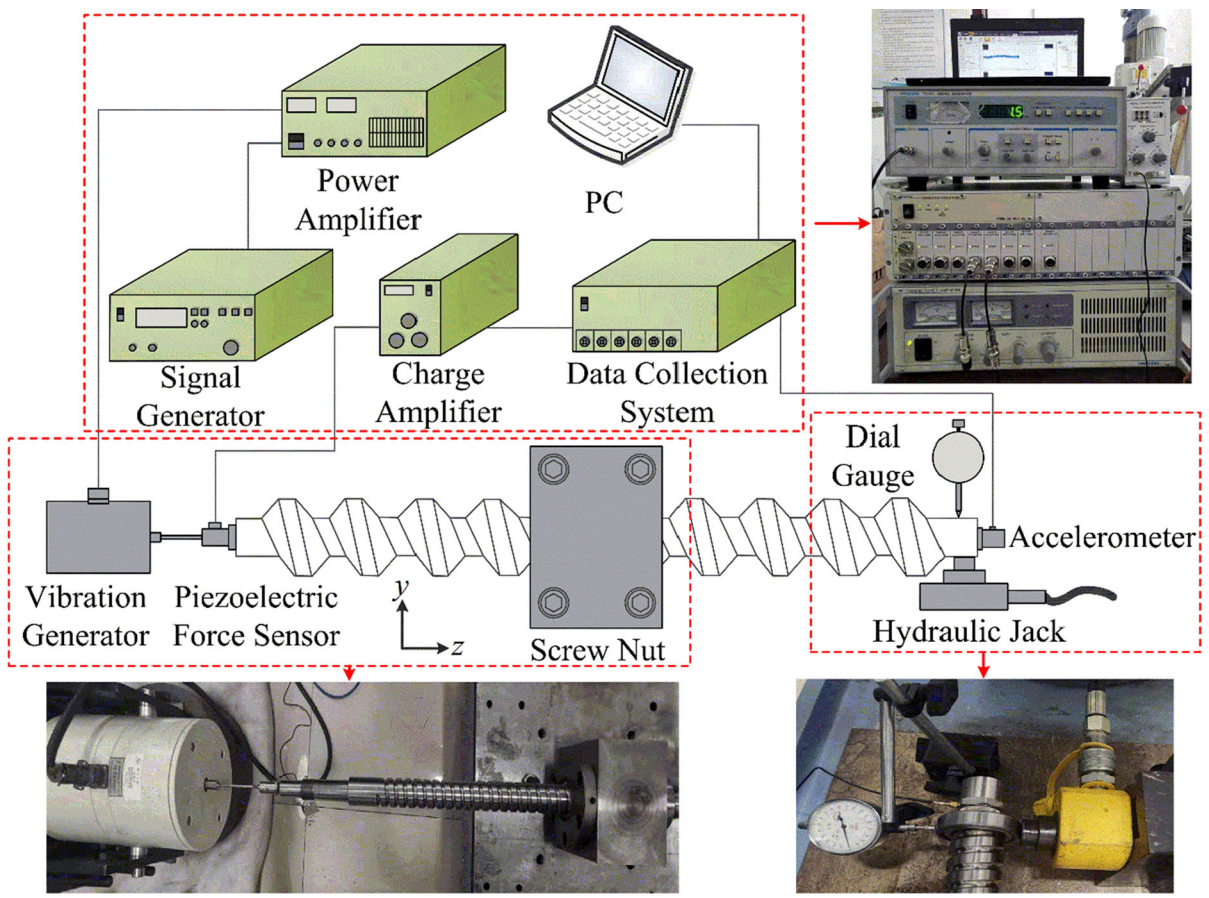

Fig. 22 Experimental setup

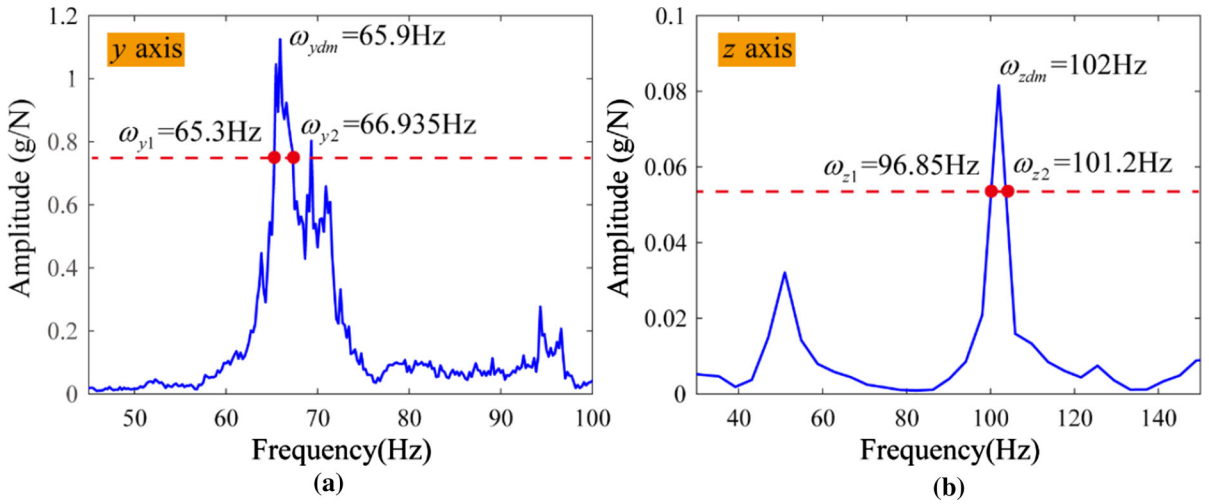

Fig. 23 Frequency response function obtained from impact test in two directions; **a** *x*-axis. **b** *z*-axis

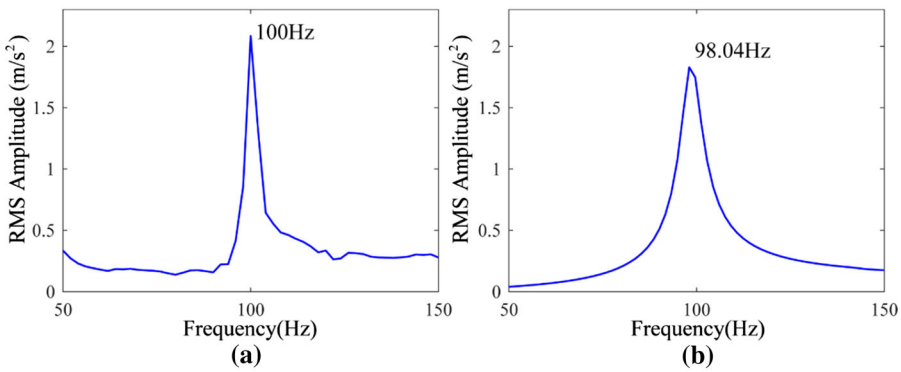

Fig. 24 Amplitude frequency curve obtained from impact test at F_0 = 50 N. **a** Experimental result. **b** Simulation result

(2) In the whole range of excitation frequency, the excitation amplitude has impacts on system dynamic response. In contrast, for other system parameters, i.e., preload and the number of balls, the influenced range of excitation frequency is relatively limited.

(3) The system parameters can affect the dynamic characteristic by different ways. Excitation amplitude and deflection angle can enhance the nonlinear properties of the system. In contrast, the preload can improve dynamics. Furthermore, the number of balls can change the resonance frequency of the system.

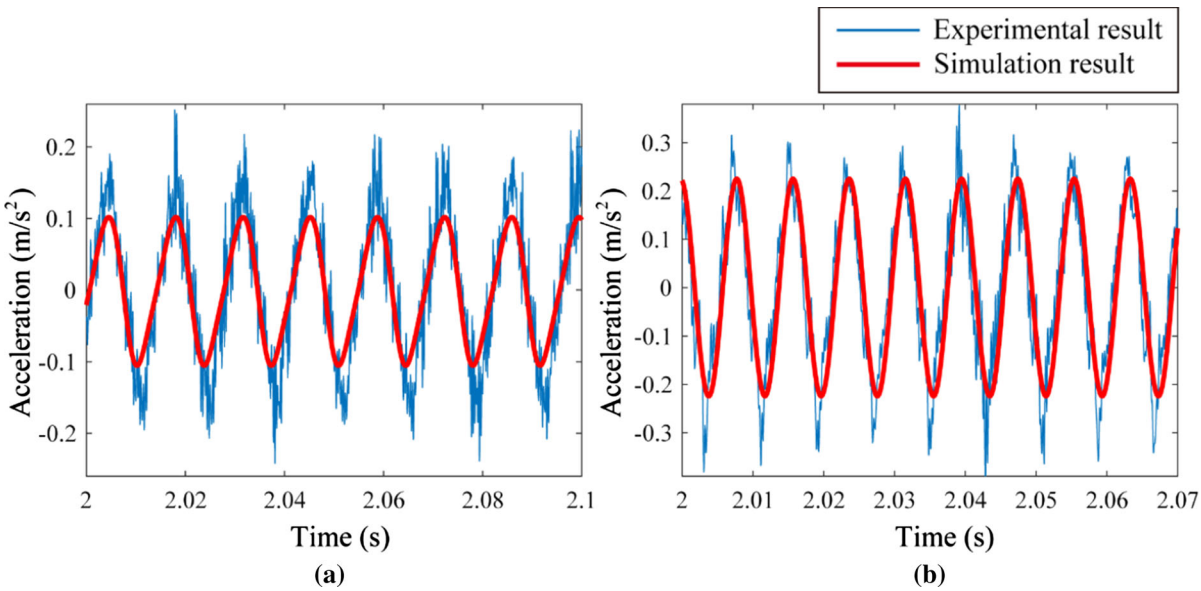

Fig. 25 Vibration response between simulation and experiment. **a** $\omega/2\pi$ = 74 Hz, F_0 = 50 N. **b** $\omega/2\pi$ = 126 Hz, F_0 = 50 N

Authors' contributions ZL contributed to methodology, investigation, experimental, writing—original draft, and writing—review and editing. MX, YZ, and HM provided resources and supervised the study. HZ contributed to resources, writing—reviewing and editing, supervision, and writing—review and editing. ZL carried out the experiment. CL and GY conceived the presented idea. CW helped in simulation and discussion. YZ provided the experimental rig.

Funding The work was supported by the National Natural Science Foundation of China (Grant No. 52075087), the Fundamental Research Funds for the Central Universities (Grant No. N2003006 and N2103003), and the National Natural Science Foundation of China (Grant No. U1708254).

Availability of data and material The datasets supporting the results of this article are included within the article and its additional files.

Declarations

Conflict of interest The authors declare that they have no known competing financial interests or personal relationships that could have appeared to influence the work reported in this paper.

Ethical approval This chapter does not contain any studies with human participants or animals performed by any of the authors.

Consent to participate Not applicable. The article involves no studies on humans.

Consent for publication All authors have read and agreed to the published version of the manuscript.

References

1. Wheeler, P., Bozhko, S.: The more electric aircraft: technology and challenges. IEEE Electrif. Mag. **2**, 6–12 (2014)
2. Kim, S.K., Cho, D.W.: Real-time estimation of temperature distribution in a ball-screw system. Int. J. Mach. Tools Manuf. **37**, 451–464 (1997)
3. Tsai, P.C., Cheng, C.C., Hwang, Y.C.: Ball screw preload loss detection using ball pass frequency. Mech. Syst. Signal Process. **48**, 77–91 (2014)
4. Xu, Z.Z., Liu, X.J., Kim, H.K., Shin, J.H., Lyu, S.K.: Thermal error forecast and performance evaluation for an air-cooling ball screw system. Int. J. Mach. Tools Manuf. **51**, 605–611 (2011)
5. Li, P., Jia, X., Feng, J., Davari, H., Qiao, G., Hwang, Y., Lee, J.: Prognosability study of ball screw degradation using systematic methodology. Mech. Syst. Signal Process. **109**, 45–57 (2018)
6. Liu, Z., Xu, M., Zhang, H., Miao, H., Li, Z., Li, C., Zhang, Y.: Nonlinear dynamic analysis of ball screw feed system considering assembly error under harmonic excitation. Mech. Syst. Signal Process. **157**, 107717 (2021)
7. Feng, G.-H., Pan, Y.-L.: Investigation of ball screw preload variation based on dynamic modeling of a preload adjustable feed-drive system and spectrum analysis of ball-nuts sensed vibration signals. Int. J. Mach. Tools Manuf. **52**, 85–96 (2012)
8. Luo, B., Pan, D., Cai, H., Mao, X., Peng, F., Mao, K., Li, B.: A method to predict position-dependent structural natural

frequencies of machine tool. Int. J. Mach. Tools Manuf **92**, 72–84 (2015)
9. Zhen, N., An, Q.: Analysis of stress and fatigue life of ball screw with considering the dimension errors of balls. Int. J. Mech. Sci. **137**, 68–76 (2018)
10. Chen, Y., Tang, W.: Dynamic contact stiffness analysis of a double-nut ball screw based on a quasi-static method. Mech. Mach. Theory **73**, 76–90 (2014)
11. Zhang, H., Zhang, J., Liu, H., Liang, T., Zhao, W.: Dynamic modeling and analysis of the high-speed ball screw feed system. Proc. Inst. Mech. Eng. Part B J. Eng. Manuf. **229**, 870–877 (2015)
12. Dong, L., Tang, W.: Hybrid modeling and analysis of structural dynamic of a ball screw feed drive system. Mechanika **19**, 316–323 (2013)
13. Wang, W., Zhou, Y., Wang, H., Li, C., Zhang, Y.: Vibration analysis of a coupled feed system with nonlinear kinematic joints. Mech. Mach. Theory **134**, 562–581 (2019)
14. Xu, M., Cai, B., Li, C., Zhang, H., Liu, Z., He, D., Zhang, Y.: Dynamic characteristics and reliability analysis of ball screw feed system on a lathe. Mech Mach Theory, 150 (2020).
15. Zhang, J., Zhang, H., Du, C., Zhao, W.: Research on the dynamics of ball screw feed system with high acceleration. Int. J. Mach. Tools Manuf. **111**, 9–16 (2016)
16. Hung, J.P., Wu, J.S.S., Chiu, J.Y.: Impact failure analysis of re-circulating mechanism in ball screw. Eng. Fail. Anal. **11**, 561–573 (2004)
17. Liao, N.T., Lin, J.F.: A new method for the analysis of deformation and load in a ball bearing with variable contact angle. J. Mech. Des. **123**, 304–312 (2001)
18. Liu, C., Zhao, C., Meng, X., Wen, B.: Static load distribution analysis of ball screws with nut position variation. Mech. Mach. Theory **151**, 103893 (2020)
19. Zhao, J., Lin, M., Song, X., Guo, Q.: Investigation of load distribution and deformations for ball screws with the effects of turning torque and geometric errors. Mech. Mach. Theory **141**, 95–116 (2019)
20. Wei, C.-C., Liou, W.-L., Lai, R.-S.: Wear analysis of the offset type preloaded ball-screw operating at high speed. Wear **292**, 111–123 (2012)
21. Okwudire, C.E., Altintas, Y.: Hybrid Modeling of Ball Screw Drives With Coupled Axial, Torsional, and Lateral Dynamics. J. Mech. Design **131**(7), 071002 (2009)
22. Zhou, C.-G., Xie, J.-L., Feng, H.-T.: Investigation of the decompression condition of double-nut ball screws considering the influence of the geometry error and additional elastic unit. Mech. Mach. Theory **156**, 104164 (2021)
23. Vicente, D.A., Hecker, R.L., Villegas, F.J., Flores, G.M.: Modeling and vibration mode analysis of a ball screw drive. Int. J. Adv. Manuf. Technol. **58**, 257–265 (2012)
24. Kolar, P., Sulitka, M., Janota, M.: Simulation of dynamic properties of a spindle and tool system coupled with a machine tool frame. Int. J. Adv. Manuf. Technol. **54**, 11–20 (2011)
25. Yu, Y., Yao, G., Wu, Z.: Nonlinear primary responses of a bilateral supported X-shape vibration reduction structure. Mech. Syst. Signal Process. **140**, 106679 (2020)
26. Yang, T., Hou, S., Qin, Z.-H., Ding, Q., Chen, L.-Q.: A dynamic reconfigurable nonlinear energy sink. J. Sound Vib. **494**, 115629 (2021)
27. Huang, X., Li, Y., Zhang, Y., Zhang, X.: A new direct second-order reliability analysis method. Appl. Math. Model. **55**, 68–80 (2018)
28. Li, C., Xu, M., He, G., Zhang, H., Liu, Z., He, D., Zhang, Y.: Time-dependent nonlinear dynamic model for linear guideway with crowning. Tribol. Int. **151**, 106413 (2020)
29. Wang, H., Li, F., Cai, Y., Liu, Y., Yang, Y.: Experimental and theoretical analysis of ball screw under thermal effect. Tribol. Int. **152**, 106503 (2020)
30. Li, T.-J., Yuan, J.-H., Zhang, Y.-M., Zhao, C.-Y.: Time-varying reliability prediction modeling of positioning accuracy influenced by frictional heat of ball-screw systems for CNC machine tools. Precis. Eng. **64**, 147–156 (2020)
31. Mi, L., Yin, G.-F., Sun, M.-N., Wang, X.-H.: Effects of preloads on joints on dynamic stiffness of a whole machine tool structure. J. Mech. Sci. Technol. **26**, 495–508 (2012)
32. Liu, J., Shao, Y., Lim, T.C.: Vibration analysis of ball bearings with a localized defect applying piecewise response function. Mech. Mach. Theory **56**, 156–169 (2012)
33. Gunduz, A., Dreyer, J.T., Singh, R.: Effect of bearing preloads on the modal characteristics of a shaft-bearing assembly: Experiments on double row angular contact ball bearings. Mech. Syst. Signal Process. **31**, 176–195 (2012)
34. Liu, J., Shao, Y.: Dynamic modeling for rigid rotor bearing systems with a localized defect considering additional deformations at the sharp edges. J. Sound Vib. **398**, 84–102 (2017)
35. Babu, C.K., Tandon, N., Pandey, R.K.: Vibration Modeling of a Rigid Rotor Supported on the Lubricated Angular Contact Ball Bearings Considering Six Degrees of Freedom and Waviness on Balls and Races. J. Vib. Acoust. Trans. Asme **134**(1), 011006 (2012)
36. Sun, W., Kong, X., Wang, B., Li, X.: Statics modeling and analysis of linear rolling guideway considering rolling balls contact. Proc. Inst. Mech. Eng. Part C J. Mech. Eng. Sci. **229**, 168–179 (2015)
37. Gu, J., Zhang, Y.: Dynamic analysis of a ball screw feed system with time-varying and piecewise-nonlinear stiffness. Proc. Inst. Mech. Eng. Part C J. Mech. Eng. Sci. **233**, 6503–6518 (2019)
38. Harris, T.A., Kotzalas, M.N.: Rolling bearing analysis: essential concepts of bearing technology, 5th edn. Taylor and Francis, NewYork (2007)
39. Bizarre, L., Nonato, F., Cavalca, K.L.: Formulation of five degrees of freedom ball bearing model accounting for the nonlinear stiffness and damping of elastohydrodynamic point contacts. Mech. Mach. Theory **124**, 179–196 (2018)
40. Tandon, N., Choudhury, A.: A review of vibration and acoustic measurement methods for the detection of defects in rolling element bearings. Tribol. Int. **32**, 469–480 (1999)
41. Gao, P., Hou, L., Yang, R., Chen, Y.: Local defect modelling and nonlinear dynamic analysis for the inter-shaft bearing in a dual-rotor system. Appl. Math. Model. **68**, 29–47 (2019)
42. Molnár, T.G., Dombóvári, Z., Insperger, T., Stépán, G.: On the analysis of the double Hopf bifurcation in machining processes via centre manifold reduction. Proc. R. Soc. A Math. Phys. Eng. Sci. **473**, 20170502 (2017)
43. Stépán, G., Haller, G.: Quasiperiodic oscillations in robot dynamics. Nonlinear Dyn. **8**, 513–528 (1995)

44. Chandra, N.H., Sekhar, A.S.: Swept sine testing of rotor-bearing system for damping estimation. J. Sound Vib. **333**, 604–620 (2014)